Principal Component Analysis of Remote Sensing of Aerosols Over Oceans

Viktor Zubko, Yoram J. Kaufman, Richard I. Burg, and J. Vanderlei Martins

***Abstract*—We apply principal component analysis (PCA) to estimate how much information about atmospheric aerosols could be retrieved from solar-reflected radiances observed over oceans by a satellite sensor as a function of the number of wavelength bands, viewing angles, and Stokes parameters. It is assumed that our virtual satellite sensor can simultaneously perform multispectral, multiangle, and linear polarization measurements of the radiances, and the following quantities are used to vary: aerosol optical thickness, single-scattering albedo (SSA) of aerosol particles, height of the aerosol layer, aerosol model (includes size distribution parameters and optical properties), and wind speed. The real refractive index was kept constant and, therefore, is not part of the analysis. To calculate the number of significant principal components (SPCs), the cumulative percent variance rule is used, which takes into account anticipated errors of measurements. The reported results predict how much additional information can be retrieved from observations by adding more wavelength, angle, and polarization channels. For example, for the Moderate Resolution Imaging Spectroradiometer instruments ($\lambda > 0.5\ \mu$m), the number of SPCs is two to three; for Multiangle Imaging SpectroRadiometer, three to five; for Polarization and Directionality of the Earth Reflectances, five to ten; while for the future Glory/Aerosol Polarization Sensor instrument, it is 6–11 (when using eight out of its > 100 view angles). The ranges reflect view conditions and analysis method. Our calculations show that the observations should be most sensitive to the aerosol model followed in decreasing order by optical thickness, SSA, and aerosol height. We found that there is no systematic increase in the information about aerosol starting from 10–15 view angles for unpolarized observations and 30 view angles for those with linear polarization. It is achievable with modern detectors to retrieve up to 10 and 16 SPCs from unpolarized and polarized observations, respectively. The methodology and results of our PCA can be useful for estimating the reliability of aerosol parameters retrieved from existing and future satellite observations.**

***Index Terms*—Aerosols, remote sensing, satellite applications.**

I. Introduction

ATMOSPHERIC aerosols interact with the Earth radiation and hydrological cycles and play an important biogeochemical role in the Earth system [1], [2]. Aerosols are liquid and solid particles suspended in the air from natural or man-made sources. They can affect human health, visibility, and climate. Aerosol particles affect climate directly by reflecting and absorbing solar and terrestrial radiation, and indirectly by their influence on cloud microphysics, albedo, and precipitation [3]–[5]. Modeling of aerosol effects shows that aerosols, via scattering solar radiation and interfering with cloud processes, should increase reflection of radiation back to space, thus having a cooling effect on the climate [6]–[8]. However, aerosols that contain black carbon particles strongly absorb the incoming sunlight. The aerosol absorption can result in the warming of the atmosphere and cooling of the surface, with subsequent reduction of the atmospheric vertical temperature gradient that, in turn, could influence the rates of evaporation and cloud development [9]–[11]. Accurate knowledge of the interplay of the radiative effects of aerosol and greenhouse gases is needed in order to measure the sensitivity of the Earth to radiative forcing and to predict climate change [12].

Aerosols have a short lifetime (of 7–10 days) and, therefore, have high spatial and temporal variability. Their interaction with solar radiation and clouds is controlled by their intrinsic properties. Therefore, to quantify the aerosol effect on climate, accurate spatial and temporal distributions of aerosol properties (composition, particle size distribution, and optical thickness, just to name a few) measured on a global scale are needed [13]. This objective can be achieved by using long-term satellites capable of sensing solar-scattered radiation for a wide range of wavelengths and viewing angles and for various polarization states, in combination with surface and aircraft measurements. Because of the vector nature of light, it is characterized by the intensity and state of polarization, which are common to express through the Stokes vector with the components, Stokes parameters: I, Q, U, and V [14]. The first, I, describes the total (polarized and unpolarized) radiance. The next two Stokes parameters, Q and U, describe the linearly polarized radiance, and the last, V, is the radiance circularly polarized. Currently flying satellite instruments measure only part of the information available in the reflected sunlight. For example, Polarization and Directionality of the Earth Reflectances (POLDER) [15] measures three Stokes parameters I, Q, and U for up to 14 viewing angles, but only in three wavelength bands centered at 0.443, 0.67, and 0.865 μm. The Moderate Resolution Imaging Spectroradiometer (MODIS) [16] measures radiances in seven wavelength bands spanning the range from 0.47–2.13 μm, but without polarization and for one viewing angle at a time. The Multiangle Imaging SpectroRadiometer (MISR) [17] measures reflected radiances in four wavelength bands ranging from

Manuscript received April 11, 2006; revised August 31, 2006. This work was supported by the National Aeronautics and Space Administration's/Glory Mission project.

V. Zubko is with RS Information Systems, Inc./Goddard Earth Sciences Data and Information Services Center, NASA Goddard Space Flight Center, Greenbelt, MD 20771 USA (e-mail: vzubko@pop600.gsfc.nasa.gov).

Y. J. Kaufman, deceased, was with the Climate and Radiation Branch, NASA Goddard Space Flight Center, Greenbelt, MD 20771 USA.

R. I. Burg is with the Earth Observing System: Program Office, NASA Goddard Space Flight Center, Greenbelt, MD 20771 USA (e-mail: Richard.Burg-1@nasa.gov).

J. V. Martins is with the Joint Center for Earth Systems Technology, University of Maryland Baltimore County, Baltimore, MD 21250 USA (e-mail: martins@climate.gsfc.nasa.gov).

Digital Object Identifier 10.1109/TGRS.2006.888138

0.44–0.86 μm for nine view angles (except exactly at the solar equator) and without polarization.

From future missions, Glory will be a remote-sensing Earth-orbiting observatory, whose main objective is to collect data on various physical and chemical properties, and spatial and temporal distributions of aerosols. The objective will be accomplished with the Glory/Aerosol Polarization Sensor (APS), which will measure three Stokes parameters I, Q, and U with a continuous scan with over 100 view angles and nine wavelengths bands (0.4–2.4 μm) [13].

A sensitivity analysis regarding polarization measurements was already reported by Mishchenko and Travis [18]–[20]. They show that remote-sensing algorithms, based on high-precision multiangle measurements of polarization and radiance at one or several wavelengths, are less dependent on *a priori* information about the aerosol than algorithms using radiance measurements alone. As a result, the polarization measurements can be used to retrieve the aerosol optical thickness (AOT), effective radius, and refractive index with very high accuracy of ± 0.015, ± 0.03 μm, and ± 0.01, respectively.

Thus, the purpose of this paper is to analyze how much information about atmospheric aerosols could be retrieved from solar reflected radiances observed by a satellite sensor as a function of the number of wavelength bands, viewing angles, and Stokes parameters. For this purpose, we use the principal component analysis (PCA), which is a well-known multivariate technique [21]. The results presented here can be useful in designing aerosol retrieval algorithms for upcoming cosmic missions devoted to aerosols. For example, the estimated number of SPCs could be used in defining the reliability weights for aerosol parameters to be retrieved. It would allow one to fine-tune the retrieval scheme: to put more attention to more reliable parameters and isolate those parameters with low reliability or not retrievable.

A signal detected by a satellite sensor contains responses of aerosol, atmospheric molecules (Rayleigh scattering), and underlying surface. Therefore, to separate the contribution of aerosol, we should be able to properly model the other contributors. As a rule, Rayleigh scattering can be predicted quite accurately. The contribution of the surface is different for the ocean and land. Because land surface has quite complex and variable reflectance properties [22], it is difficult to model its contribution at a global scale. In contrast, the ocean surface albedo is relatively low and constant [23], and this should simplify the modeling process. Therefore, the work reported in this paper has been carried out for oceans only.

It is worth noting that Tanré *et al.* [24] already used the PCA to estimate the information on aerosol parameters contained in the reflected solar radiances detected over oceans in the 0.53–2.2-μm range. The authors found that only one to two parameters of the size distribution could be retrieved. The computations were performed for the MODIS spectral bands with one viewing angle. Two parameters of a lognormal size distribution, the effective radius and width of the distribution, were identified as the key variables. Here, we are expanding the analysis of the study in [24], that is, we use the vector radiative transfer calculations for the system of atmosphere (aerosol and molecules) and ocean to get the radiances for a number of viewing directions, wavelengths, and polarization states suitable for aerosol space sensors. We also use a broader set of aerosol-related quantities as variables, such as particle size distribution and optical parameters, optical thickness of the aerosol layer, single-scattering albedo (SSA) of aerosol particles, height of the aerosol layer, and wind speed.

TABLE I
AEROSOL MODEL PARAMETERS

Parameter	#	Values
Modes	2	Fine, Course
Models	6	1-4 (Fine), 8-9 (Course)
Layer Height (km)	4	0-1, 1-2, 2-3, 3-4
Optical Thickness	4	0, 0.1, 0.2, 0.3, 0.5
Single Scattering Albedo	4	0.75, 0.85, 0.95, 1
Wind Speed (km s^{-1})	4	2, 4, 6, 8

Our modeling approach is described in Section II, the results can be found in Section III, and Section IV concludes the paper.

II. MODELING APPROACH

To proceed with modeling, we should first define the main aerosol parameters and a set of their values for variation, together with the scattering properties of the atmosphere and ocean. At the next step, we calculate a lookup table of the top-of-atmosphere reflectances for the set of predefined parameters. Finally, we perform the PCA of the reflectances and find the number of SPCs. Below, we describe all these topics in detail.

A. Aerosol Parameters

The following aerosol parameters were used as variables in our PCA.

1) SSA is a ratio of aerosol scattering coefficient to the total aerosol extinction (scattering + absorption) coefficient. We did calculations for the several values of SSA from 0.75 to 1 (Table I).
2) AOT is an index of the attenuation of radiation as it passes through the atmosphere, due to the presence of suspended aerosol particles. Usually, it defines at the wavelength at or around 0.55 μm. We did calculations for several values of AOT between 0 and 0.5 (Table I).
3) Aerosol layer height. We assume that the aerosol layer has the vertical size of 1 km and the layer base height varies between 0 and 3 km (Table I).
4) Aerosol size distribution model. We base our PCA calculations on six various aerosol particle size distribution models (Tables I and II) from which models 1–4 correspond to the fine mode (small particles) and models 8–9 correspond to the coarse mode (big particles). The model running numbers correspond to the respective models from the study in [25] used for MODIS aerosol retrievals. We assume that each model obeys a lognormal size distribution

$$n(R) = \frac{N}{2.3R\sigma_g\sqrt{2\pi}} \exp\left\{-\frac{(\log R - \log R_g)^2}{2\sigma_g^2}\right\} \quad (1)$$

where N is the total particle number density, R_g is the median radius, and σ_g is the standard deviation of $\log R$.

TABLE II
AEROSOL MODEL OPTICAL PROPERTIES. R_g, R_{eff}, AND σ_g ARE THE MEDIAN RADIUS, THE EFFECTIVE RADIUS, AND THE STANDARD DEVIATION OF LOGARITHM OF THE PARTICLE RADIUS FOR A LOGNORMAL SIZE DISTRIBUTION. ω_o IS THE SSA. MODELS 1–2 ARE WET WATER SOLUBLE TYPE. MODELS 3–4 ARE WATER SOLUBLE WITH HUMIDITY, AND MODELS 8–9 ARE DUSTLIKE TYPE

Mode	Model	Size Distribution R_g (μm)	σ_g	R_{eff} (μm)	ω_o	Optical Constants: n and k λ (μm) 0.340	0.411	0.533	0.644	0.855	1.243	1.632	2.119
Fine	1	0.07	0.4	0.10	0.75	$1.45_{0.052}$	$1.45_{0.046}$	$1.45_{0.0368}$	$1.45_{0.029}$	$1.45_{0.0179}$	$1.45_{0.0079}$	$1.43_{0.0095}$	$1.43_{0.0054}$
					0.85	$1.45_{0.028}$	$1.45_{0.025}$	$1.45_{0.0198}$	$1.45_{0.0158}$	$1.45_{0.0092}$	$1.45_{0.00473}$	$1.43_{0.0039}$	$1.43_{0.0019}$
					0.95	$1.45_{0.0081}$	$1.45_{0.0067}$	$1.45_{0.0056}$	$1.45_{0.0046}$	$1.45_{0.0029}$	$1.45_{0.0013}$	$1.43_{0.0006}$	$1.40_{0.00025}$
					1.00	$1.45_{0.0}$	$1.45_{0.0}$	$1.45_{0.0}$	$1.45_{0.0}$	$1.45_{0.0}$	$1.45_{0.0}$	$1.43_{0.0}$	$1.40_{0.0}$
	2	0.06	0.6	0.15	0.75	$1.45_{0.0544}$	$1.45_{0.052}$	$1.45_{0.0499}$	$1.45_{0.0450}$	$1.45_{0.0364}$	$1.45_{0.025}$	$1.43_{0.036}$	$1.40_{0.0182}$
					0.85	$1.45_{0.027}$	$1.45_{0.028}$	$1.45_{0.0251}$	$1.45_{0.024}$	$1.45_{0.02}$	$1.45_{0.0123}$	$1.43_{0.0129}$	$1.40_{0.0075}$
					0.95	$1.45_{0.008}$	$1.45_{0.008}$	$1.45_{0.0077}$	$1.45_{0.0072}$	$1.45_{0.0059}$	$1.45_{0.0039}$	$1.43_{0.0022}$	$1.40_{0.0012}$
					1.00	$1.45_{0.0}$	$1.45_{0.0}$	$1.45_{0.0}$	$1.45_{0.0}$	$1.45_{0.0}$	$1.45_{0.0}$	$1.43_{0.0}$	$1.40_{0.0}$
	3	0.08	0.6	0.20	0.75	$1.45_{0.051}$	$1.40_{0.049}$	$1.40_{0.0475}$	$1.40_{0.0453}$	$1.40_{0.038}$	$1.40_{0.028}$	$1.39_{0.045}$	$1.36_{0.0255}$
					0.85	$1.45_{0.0233}$	$1.40_{0.0235}$	$1.40_{0.0245}$	$1.40_{0.024}$	$1.40_{0.02}$	$1.40_{0.0155}$	$1.39_{0.018}$	$1.36_{0.011}$
					0.95	$1.45_{0.0071}$	$1.40_{0.0074}$	$1.40_{0.0074}$	$1.40_{0.0071}$	$1.40_{0.0062}$	$1.40_{0.0044}$	$1.39_{0.003}$	$1.36_{0.016}$
					1.00	$1.45_{0.0}$	$1.40_{0.0}$	$1.40_{0.0}$	$1.40_{0.0}$	$1.40_{0.0}$	$1.40_{0.0}$	$1.39_{0.0}$	$1.36_{0.0}$
	4	0.10	0.6	0.24	0.75	$1.45_{0.0479}$	$1.40_{0.0481}$	$1.40_{0.0483}$	$1.40_{0.0478}$	$1.40_{0.0430}$	$1.40_{0.034}$	$1.39_{0.06}$	$1.36_{0.037}$
					0.85	$1.45_{0.022}$	$1.40_{0.023}$	$1.40_{0.025}$	$1.40_{0.025}$	$1.40_{0.022}$	$1.40_{0.0193}$	$1.39_{0.023}$	$1.36_{0.015}$
					0.95	$1.45_{0.00652}$	$1.40_{0.0072}$	$1.40_{0.0074}$	$1.40_{0.0074}$	$1.40_{0.0069}$	$1.40_{0.0055}$	$1.39_{0.004}$	$1.36_{0.025}$
					1.00	$1.45_{0.0}$	$1.40_{0.0}$	$1.40_{0.0}$	$1.40_{0.0}$	$1.40_{0.0}$	$1.40_{0.0}$	$1.39_{0.0}$	$1.36_{0.0}$
Coarse	8	0.6	0.6	1.46	0.75	$1.45_{0.0081}$	$1.53_{0.0097}$	$1.53_{0.0127}$	$1.53_{0.0151}$	$1.53_{0.02}$	$1.46_{0.032}$	$1.46_{0.1458}$	$1.46_{0.151}$
					0.85	$1.45_{0.037}$	$1.53_{0.043}$	$1.53_{0.0056}$	$1.53_{0.0068}$	$1.53_{0.009}$	$1.46_{0.0146}$	$1.46_{0.0404}$	$1.46_{0.047}$
					0.95	$1.45_{0.001}$	$1.53_{0.0012}$	$1.53_{0.00145}$	$1.53_{0.00177}$	$1.53_{0.0025}$	$1.46_{0.004}$	$1.46_{0.0049}$	$1.46_{0.006}$
					1.00	$1.45_{0.0}$	$1.53_{0.0}$	$1.53_{0.0}$	$1.53_{0.0}$	$1.53_{0.0}$	$1.46_{0.0}$	$1.46_{0.0}$	$1.46_{0.0}$
	9	0.5	0.8	2.36	0.75	$1.45_{0.00587}$	$1.53_{0.0069}$	$1.53_{0.0091}$	$1.53_{0.01092}$	$1.53_{0.01399}$	$1.46_{0.0213}$	$1.46_{0.1276}$	$1.46_{0.13}$
					0.85	$1.45_{0.0023}$	$1.53_{0.003}$	$1.53_{0.0039}$	$1.53_{0.0047}$	$1.53_{0.0064}$	$1.46_{0.0096}$	$1.46_{0.027}$	$1.46_{0.034}$
					0.95	$1.45_{0.0008}$	$1.53_{0.0008}$	$1.53_{0.00099}$	$1.53_{0.00125}$	$1.53_{0.00165}$	$1.46_{0.0024}$	$1.46_{0.0033}$	$1.46_{0.0043}$
					1.00	$1.45_{0.0}$	$1.53_{0.0}$	$1.53_{0.0}$	$1.53_{0.0}$	$1.53_{0.0}$	$1.46_{0.0}$	$1.46_{0.0}$	$1.46_{0.0}$

The parameters R_g and σ_g of the models are presented in Table II. We further assume that each of the six models can have submodels corresponding to several values of the SSA from 0.75 to 1 (Table I). The optical constants for each aerosol model and SSA are presented in Table II.

Note, however, that our analysis does not include the nonsphericity of aerosols, which could increase the uncertainty of our PCA results for models of dustlike particles [26]. In addition, due to our choice of the optical model of aerosols, we do not use refractive index as a directly varied parameter. Instead, the refractive index is incorporated into the parameter called aerosol model.

B. Simulated Top-of-Atmosphere Reflectances

We calculated the top-of-atmosphere reflectances at eight wavelengths spanning the range 0.34–2.119 μm: six from them (0.533–2.119 μm) approximately correspond to respective MODIS bands [15]. We added two more wavelengths into our analysis: in blue (0.411 μm) and ultraviolet (0.34 μm) in order to estimate how much information about aerosols this can provide.

The top-of-atmosphere reflectances for the lookup table were computed for the above set of aerosol parameters and for an array of angles using the radiative transfer code of Ahmad and Fraser [27]. It fully suits our needs: 1) includes the polarization effects; 2) takes into account light scattering by molecules (Rayleigh scattering) and aerosol particles; and 3) considers reflection of light by the ocean surface. The ocean reflection has several contributors such as the Fresnel reflection by the rough ocean (Sun glitter) [28], reflection by foam [29], and the Lambertian reflection by underwater scattering elements (sediments, pigments, etc.). For simplicity, we assumed zero water leaving radiance. Typically, its contribution to the total observed radiance is at most 10% in blue, and less than 5% in green [30]. Because we work in this paper on the aerosol reflectance (see this section below), a difference between the reflectances from the same scene with and without aerosol, we therefore expect that the error in the aerosol reflectance due to the assumption of zero water leaving radiance should not be large. We reserved up to 5% for the error in our PCA (see Section II-D below). The percentage of the ocean surface occupied by foam depends on the wind speed [29]. For the lookup table, reflectances were calculated for several values of the wind speed from 2–8 m s^{-1} (Table I).

Therefore, the top-of-atmosphere reflectance is a function of a number of parameters: $\rho(\lambda, i_{\text{pol}}, \theta_{\text{in}}, \theta_{\text{out}}, \Phi_{\text{out}}; m, H, \omega_o, \tau, \nu)$, where parameters of the first group characterize conditions of observations and parameters of the second group describe the aerosol properties: λ is the wavelength, i_{pol} is the index of the respective Stokes parameter ($i_{\text{pol}} = 1$–4 for I, Q, U, and V, respectively), θ_{in} is the solar zenith angle, θ_{out} is the view zenith angle, Φ_{out} is the view azimuth angle, m is the index of the aerosol size distribution model, H is the aerosol layer height, ω_o is the SSA, τ is the aerosol layer optical thickness, and ν is the over-ocean wind speed. To scale down the contributions of the atmosphere and ocean reflection while doing PCA, we used the aerosol reflectance instead of original reflectance: $\Delta\rho(\tau) = \rho(\tau) - \rho(\tau = 0)$, that is a difference of the reflectances corresponding to the cases of with and without

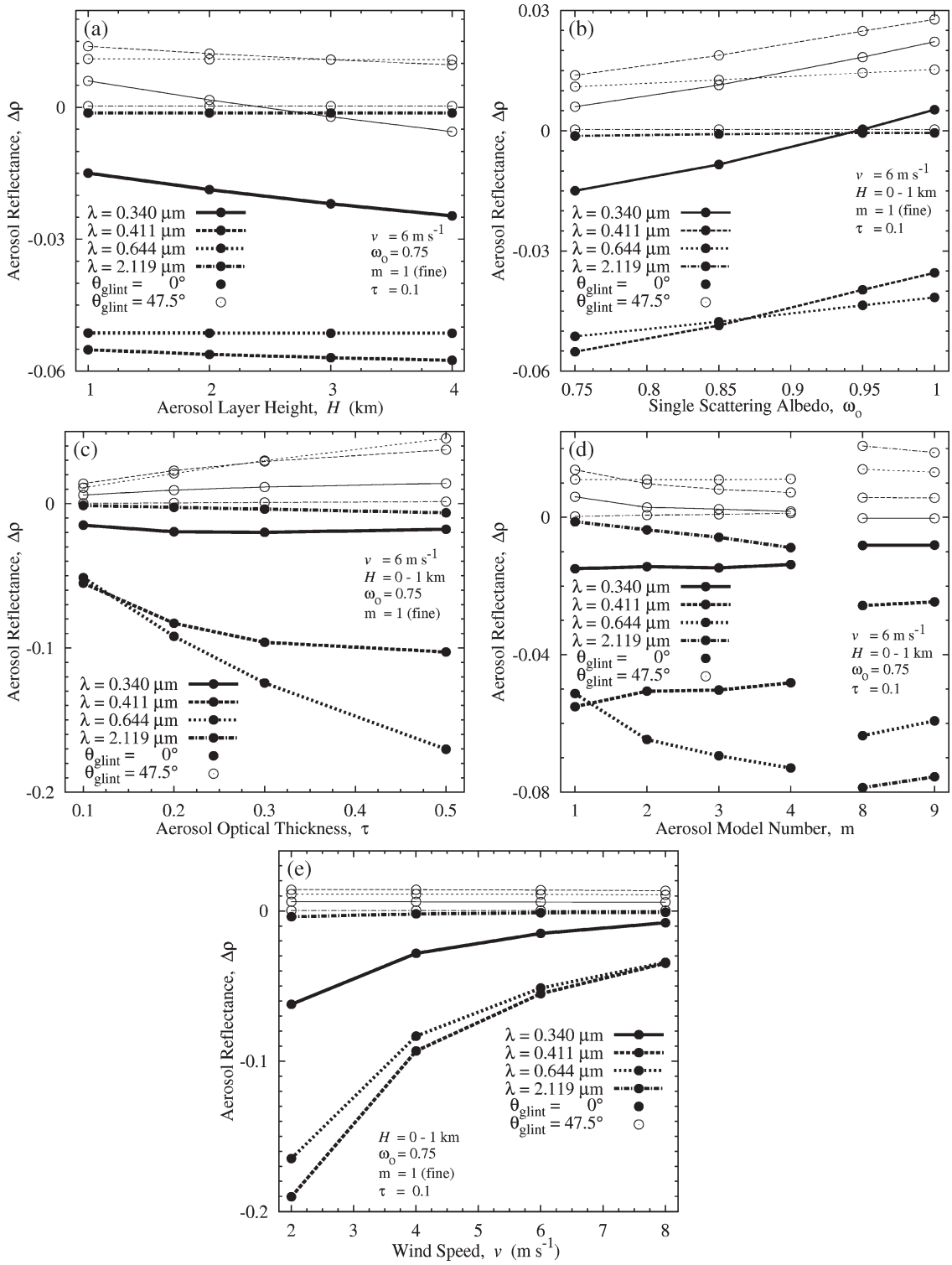

Fig. 1. Typical aerosol reflectances as a function of (a) aerosol layer height, (b) SSA, (c) AOT, (d) aerosol model number, and (e) wind speed.

aerosol. Typical dependences of aerosol reflectances on various aerosol parameters are shown in Fig. 1.

C. Basics of the PCA

PCA is a multivariate technique that allows us to reduce an original set of correlated observed variables into a smaller set of uncorrelated rather artificial variables called principal components (PCs), each of which is a particular linear combination of the original variables [21]. Thus, the purpose of PCA is to achieve parsimony and reduce dimensionality by finding the smallest number of components that explain most of the variation in the original data and to summarize the data with little loss of information. The PCs are extracted in decreasing order of importance so that the first PC accounts for as much of the variation as possible and each successive component accounts

for a little less. To restore the total system variability of the original variables, we need all PCs. However, if the first few PCs explain a large proportion of the variability (usually 90%–95%), our purpose of dimension reduction has been achieved. Because PCA is just a mathematical technique, the interpretation of PCs is neither easy nor straightforward, in general [31].

Note the limitation of the PCA. The technique is linear; therefore, any nonlinear correlation between variables will not be captured. However, generally, the dependences of our aerosol reflectances on aerosol parameters do not deviate much from linear ones (see Fig. 1). Thus, we think that the influence of the nonlinearities on our PCA results is small. To get a quantitative measure of the influence, a nonlinear approach, for example, nonlinear PCA on the base of the neural network models [32] or independent component analysis [33], should be used, but this is beyond the scope of this paper.

The following is a detailed description of the algorithm we used for the PCA of the aerosol reflectances.

Step 1) Organize the input data, top-of-atmosphere reflectances ρ, into a matrix $\mathbf{D}_0$ with the number of columns n_o and with the number of rows n_a. Number n_o corresponds to the number of observational data that is equal to $n_\lambda \cdot n_\theta \cdot n_s$, where n_λ is the number of wavelengths, n_θ is the number of viewing directions, and n_s is the number of Stokes parameters ($n_s = 1$ for observations without polarization and $n_s = 3$ with linear polarization). Number n_a corresponds to the number of aerosol models that is equal to $n_H \cdot n_\omega \cdot n_\tau \cdot n_m \cdot n_\nu$, where n_H is the number of aerosol layer heights, n_ω is the number of SSAs, n_τ is the number of AOTs, n_m is the number of aerosol particle size distributions, and n_ν is the number of wind speeds. Therefore, the total number of matrix elements is $n_o \cdot n_a$, and the relation $n_a \geq n_o$ should hold for PCA to work.

Step 2) Form a matrix $\mathbf{D}_1$ with aerosol reflectances $\Delta\rho$ as $\mathbf{D}_1 = \mathbf{D}_0 - \mathbf{D}_{\tau=0}$, where matrix $\mathbf{D}_{\tau=0}$ is similar to $\mathbf{D}_0$ except that all matrix elements are calculated for $\tau = 0$; that is for the case of no aerosol.

Step 3) Standardize matrix $\mathbf{D}_1$: Find the mean value $D_{1,\langle i\rangle j}$ and the standard deviation $\sigma_{1,\langle i\rangle j}$ along each column i of $\mathbf{D}_1$; then form a matrix $\mathbf{D}_2 : D_{2,ij} = (D_{1,ij} - D_{1,\langle i\rangle j})/\sigma_{1,\langle i\rangle j}$ which has zero mean and unit standard deviation for each column; this is equivalent to using the correlation matrix.

Step 4) Compute a singular value decomposition [34] for the matrix $\mathbf{D}_2$, as $\mathbf{D}_2 = \mathbf{ULV}'$, where $\mathbf{U}$ is a column-orthogonal matrix of same dimension as $\mathbf{D}_2(n_a \cdot n_o)$, $\mathbf{L}$ is a diagonal matrix $(n_o \cdot n_o)$, and $\mathbf{V}$ is an orthogonal square matrix $(n_o \cdot n_o)$. The diagonal elements of $\mathbf{L}$ (l_k, $k = 1$ to n_o) are square roots of the eigenvalues of the correlation matrix $\mathbf{D}_2'\mathbf{D}_2$. The columns of $\mathbf{V}$ are the corresponding eigenvectors (PCs) of $\mathbf{D}_2'\mathbf{D}_2$. Therefore, we can write for each matrix element $D_{2,ij}$

$$D_{2,ij} = \sum_{k=1}^{n_o} l_k U_{ik} V_{jk}. \tag{2}$$

Elements l_k measure the amount of the variation explained by each PC and will be largest for the first PC and smaller for the subsequent PCs. Eigenvectors V_{jk} provide the weights to compute the uncorrelated PCs, which are the linear combinations of the standardized original variables.

Step 5) Find the number $n_{\rm pc}$ of SPCs using a given stopping rule (we discuss these rules below). Then, we can approximate the matrix elements of $\mathbf{D}_2$ by $n_{\rm pc}$ PCs as

$$\tilde{D}_{2,ij}(n_{\rm pc}) \approx \sum_{k=1}^{n_{\rm pc}} l_k U_{ik} V_{jk}. \tag{3}$$

Step 6) Compute the approximation to the matrix elements of the original matrix $\mathbf{D}_0$ by reversing Steps 3) and 2)

$$\tilde{D}_{0,ij}(n_{\rm pc}) = D_{\tau=0,ij} + D_{1,\langle i\rangle j} + \sigma_{1,\langle i\rangle j}\tilde{D}_{2,ij}(n_{\rm pc}). \tag{4}$$

D. How to Choose the Number of SPCs?

The complete set of PCs contains the same information as the raw data. However, the data are affected by noise. Therefore, an important issue in doing a PCA is to choose the adequate number of PCs to represent the system meaningfully, with the rest of the PCs to be considered spurious. Because the nature of the decision is rather arbitrary, there is no universal stopping rule. However, a number of guidelines have been developed. The following three simple rules are commonly used [35].

1) The Kaiser–Guttman rule is one of the most used stopping rules [36], [37]. This approach accepts all PCs with eigenvalues above the average eigenvalue, which is 1.0 for correlation-based PCA like ours, and rejects those below the average (1.0). This is because any PC that displays an eigenvalue above 1.0 is accounting for a greater amount of variance than is contributed by one variable; therefore, it is worthy of being retained. On the other hand, a PC with an eigenvalue less than 1.0 is accounting for less variance than is contributed by one variable, and therefore, it is insignificant. Note that Tanré *et al.* [24] used this rule in their PCA.
2) Cumulative percent variance (CPV) [21] is a measure of the percent variance captured by the first $n_{\rm pc}$ PCs. With this rule, one selects a desired CPV, for example 90%. While the target is to explain as much of the variance as possible, one wants to retain as few PCs as possible. Thus, the decision is a balance between the amount of parsimony and comprehensiveness of the model.
3) The scree rule [38], [39] considers the eigenvalues associated with each PC against their rank order. Usually, the magnitude of successive eigenvalues drops off sharply and then tends to level off. The recommendation is to retain all eigenvalues including the first one on the line where they start to level off. Often the scree rule is complicated by either the lack of any obvious break or the possibility of multiple break points.

During the course of this paper, we experimented with all the above rules. To choose the right rule, we first calculated three

TABLE III

NUMBER OF SPCS: SPECTRAL DEPENDENCE. THE RESULTS HAVE BEEN DERIVED WITH THE CPV RULE WITH THE CRITICAL CPV = 90%. n_θ IS THE NUMBER OF VIEWING DIRECTIONS COVERING $\theta_{\rm out} = 0^\circ - 72^\circ$. n_λ IS THE NUMBER OF WAVELENGTH BANDS. λ REFLECTS THE RANGE OF THE WAVELENGTHS. n_I (n_P) IS THE NUMBER OF PCS FOR THE CASE OF NO POLARIZATION (LINEAR POLARIZATION: THREE STOKES COMPONENTS). $n_{\rm PC}$ IS THE NUMBER OF SPCS. $\nu = 6\ {\rm m \cdot s^{-1}}$ $(\nu = 2{-}8\ {\rm m \cdot s^{-1}})$ MARKS THE CASE WITH FIXED (VARIED) WIND SPEED. I (P) MARKS THE CASE OF NO (LINEAR) POLARIZATION. GL MARKS THE CASE WHEN ONE VIEWING DIRECTION IS IN GLINT: $\Phi_{\rm out} = 0^\circ/180^\circ$. OG MARKS THE CASE WHEN ALL VIEWING DIRECTIONS ARE OFF GLINT: $\Phi_{\rm out} = 48^\circ/132^\circ$. THE SOLAR ZENITH ANGLE FOR ALL THE CASES IS 48°. A SUBSCRIPT AFTER THE NUMBER OF SPCS IS THE RELATIVE CONTRIBUTION TO THE VARIANCE

n_θ	n_λ	λ (μm)	$n_{\rm I}$	$n_{\rm P}$	$n_{\rm PC}$							
					v = 6 m s^{-1}				v = 2 - 8 m s^{-1}			
					GL		OG		GL		OG	
					I	P	I	P	I	P	I	P
1	1	0.533	1	3	$1_{1.00}$	$2_{0.95}$	$1_{1.00}$	$2_{0.97}$	$1_{1.00}$	$2_{0.97}$	$1_{1.00}$	$2_{0.97}$
	2	0.533 - 0.644	2	6	$1_{0.90}$	$3_{0.95}$	$2_{1.00}$	$2_{0.91}$	$1_{0.91}$	$3_{0.95}$	$2_{1.00}$	$2_{0.91}$
	3	0.533 - 0.855	3	9	$2_{0.97}$	$3_{0.92}$	$2_{0.98}$	$3_{0.93}$	$2_{0.99}$	$3_{0.92}$	$2_{0.98}$	$3_{0.93}$
	4	0.411 - 0.855	4	12	$2_{0.90}$	$4_{0.93}$	$2_{0.94}$	$4_{0.92}$	$2_{0.94}$	$4_{0.94}$	$2_{0.94}$	$4_{0.91}$
	6	0.533 - 2.119	6	18	$2_{0.92}$	$4_{0.93}$	$2_{0.93}$	$4_{0.91}$	$2_{0.94}$	$4_{0.93}$	$2_{0.93}$	$4_{0.91}$
	7	0.411 - 2.119	7	21	$2_{0.90}$	$4_{0.91}$	$2_{0.90}$	$5_{0.90}$	$2_{0.91}$	$4_{0.90}$	$2_{0.90}$	$5_{0.90}$
	8	0.340 - 2.119	8	24	$3_{0.93}$	$5_{0.92}$	$3_{0.94}$	$6_{0.92}$	$3_{0.94}$	$5_{0.91}$	$3_{0.94}$	$6_{0.92}$
2	1	0.533	2	6	$2_{1.00}$	$3_{0.90}$	$1_{0.91}$	$2_{0.90}$	$2_{1.00}$	$4_{0.93}$	$1_{0.91}$	$2_{0.90}$
	2	0.533 - 0.644	4	12	$2_{0.93}$	$4_{0.92}$	$2_{0.90}$	$3_{0.91}$	$2_{0.94}$	$4_{0.90}$	$2_{0.90}$	$3_{0.91}$
	3	0.533 - 0.855	6	18	$3_{0.96}$	$5_{0.93}$	$2_{0.90}$	$4_{0.93}$	$3_{0.96}$	$5_{0.91}$	$3_{0.97}$	$4_{0.93}$
	4	0.411 - 0.855	8	24	$4_{0.96}$	$6_{0.91}$	$3_{0.92}$	$5_{0.92}$	$4_{0.96}$	$7_{0.92}$	$3_{0.92}$	$5_{0.92}$
	6	0.533 - 2.119	12	36	$3_{0.90}$	$5_{0.91}$	$3_{0.94}$	$5_{0.92}$	$4_{0.94}$	$6_{0.91}$	$3_{0.94}$	$5_{0.91}$
	7	0.411 - 2.119	14	42	$4_{0.91}$	$7_{0.91}$	$3_{0.91}$	$6_{0.92}$	$4_{0.92}$	$8_{0.92}$	$3_{0.90}$	$6_{0.90}$
	8	0.340 - 2.119	16	48	$5_{0.92}$	$8_{0.92}$	$4_{0.93}$	$7_{0.92}$	$5_{0.92}$	$9_{0.92}$	$4_{0.93}$	$7_{0.92}$
4	1	0.533	4	12	$3_{0.97}$	$5_{0.91}$	$2_{0.97}$	$3_{0.92}$	$3_{0.93}$	$6_{0.93}$	$2_{0.94}$	$3_{0.90}$
	2	0.533 - 0.644	8	24	$3_{0.93}$	$6_{0.92}$	$2_{0.90}$	$4_{0.92}$	$4_{0.95}$	$7_{0.92}$	$3_{0.94}$	$5_{0.93}$
	3	0.533 - 0.855	12	36	$4_{0.94}$	$6_{0.91}$	$3_{0.96}$	$4_{0.91}$	$4_{0.90}$	$7_{0.90}$	$3_{0.93}$	$5_{0.92}$
	4	0.411 - 0.855	16	48	$5_{0.93}$	$8_{0.91}$	$3_{0.91}$	$6_{0.91}$	$6_{0.94}$	$9_{0.90}$	$4_{0.93}$	$7_{0.91}$
	6	0.533 - 2.119	24	72	$4_{0.91}$	$7_{0.93}$	$3_{0.94}$	$5_{0.92}$	$5_{0.90}$	$8_{0.92}$	$3_{0.91}$	$6_{0.91}$
	7	0.411 - 2.119	28	84	$5_{0.90}$	$8_{0.91}$	$3_{0.90}$	$7_{0.91}$	$6_{0.90}$	$10_{0.91}$	$4_{0.92}$	$8_{0.91}$
	8	0.340 - 2.119	32	96	$6_{0.92}$	$9_{0.90}$	$4_{0.93}$	$8_{0.92}$	$7_{0.92}$	$11_{0.91}$	$5_{0.93}$	$9_{0.91}$
8	1	0.533	8	24	$4_{0.95}$	$6_{0.90}$	$3_{0.94}$	$4_{0.91}$	$4_{0.92}$	$7_{0.91}$	$3_{0.93}$	$5_{0.91}$
	2	0.533 - 0.644	16	48	$4_{0.92}$	$7_{0.91}$	$3_{0.91}$	$5_{0.91}$	$5_{0.93}$	$8_{0.91}$	$4_{0.93}$	$6_{0.92}$
	3	0.533 - 0.855	24	72	$5_{0.93}$	$7_{0.91}$	$3_{0.90}$	$5_{0.90}$	$6_{0.92}$	$9_{0.91}$	$4_{0.92}$	$6_{0.90}$
	4	0.411 - 0.855	32	96	$6_{0.91}$	$9_{0.91}$	$4_{0.94}$	$7_{0.90}$	$7_{0.90}$	$10_{0.90}$	$5_{0.91}$	$8_{0.90}$
	6	0.533 - 2.119	48	144	$6_{0.93}$	$8_{0.92}$	$4_{0.92}$	$6_{0.92}$	$7_{0.92}$	$9_{0.90}$	$5_{0.92}$	$7_{0.91}$
	7	0.411 - 2.119	56	168	$7_{0.91}$	$10_{0.92}$	$5_{0.92}$	$8_{0.90}$	$8_{0.91}$	$11_{0.90}$	$6_{0.92}$	$9_{0.90}$
	8	0.340 - 2.119	64	192	$8_{0.92}$	$11_{0.91}$	$5_{0.91}$	$9_{0.91}$	$9_{0.92}$	$12_{0.90}$	$6_{0.91}$	$10_{0.90}$

various versions of Table III, our principal table, by using each of the rules. Then, we checked the entries of each table with the following tests.

1) *Uniqueness:* solution should be clearly identifiable and be unique.
2) *Physical sense:* the percentage of variance due to noise provided with the solution should be consistent with the expected uncertainty of the observed reflectance.
3) *Informational sense:* when a new channel is added, we expect to have the number of SPCs greater than or equal to that at the previous state.

The testing showed that rule 3) does not pass the uniqueness test. It is hard to distinguish the solution because of the too complex behavior of the eigenvalue plots, especially when we analyze the polarization data, or simply because it is hard to identify the transition point [like in Fig. 2(a)]. Rule 1) passes tests 1) and 3), but failed in test 2) in about 40% of the table entries, when it leads to the retention of too few SPCs, which sometimes explain just 50%–60% of the variance with the rest 40%–50% would be due to noise. The latter numbers look too large. Major contributors to the uncertainty of the observed reflectance are the calibration error, which is typically 1%–4%, and the underwater radiance error, which can be up to 5%. Therefore, the total error of 5%–10% should be more realistic. We found that rule 2), the CPV rule, with CPV of 90%–95% passes all the tests. Thus, to be consistent with anticipated errors of measurements, we performed the PCA for this paper with the CPV 90% and 95% rule.

Note that we assumed the measurement error for the polarized components Q and U to be of similar level as for the radiance I, while it can be smaller [13]. However, the CPV rule we employed can only take the largest error that is the one for I into account. Therefore, the number of SPCs we received for the polarization cases $(I + Q + U)$ should be considered as lower estimates. We tried to work with more sophisticated stopping rules, which explicitly take into account specific values of errors for each piece of data and thus are able to provide more accurate estimates for the number of SPCs than the CPV rule: the χ^2 rule [40] and the eigenvalue uncertainty rule [41]. However, while physically more justified, the rules failed to pass test 3): They are unstable regarding the informational sense. Thus, we decided not to use them at least in this paper.

III. RESULTS

We have carried out the PCA for various sets of aerosol-related parameters such as particle size distribution and particle optical constants (referred to below as aerosol model or model), optical thickness of the aerosol layer τ, SSA of aerosol particles

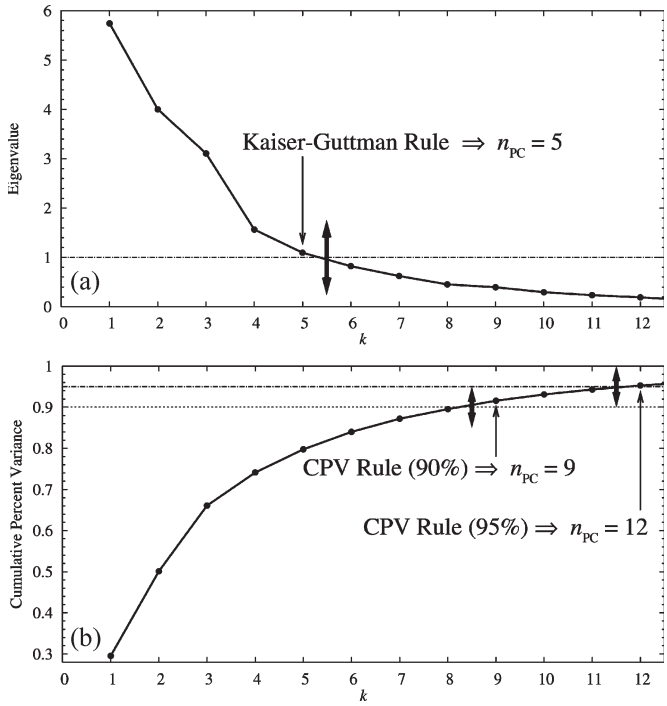

Fig. 2. Stopping rules for finding the number of SPCs. The results correspond to the model when all aerosol parameters are varied, $n_\lambda = 8$, $n_\theta = 8$, $\Phi_{\rm out} = 0^\circ/180^\circ$, and no polarization. (a) Kaiser–Guttman rule. (b) CPV rule for two values of the CPV: 90% and 95%.

ω_o, height of the aerosol layer H, and wind speed ν. We ran PCA by varying all or some of the parameters (with the rest keep fixed). For example, we fixed the wind speed to concentrate on the influence of the aerosol. Various observation situations were simulated

1) The number of wavelength bands n_λ was from one to eight, covering the range 0.340–2.119 μm.
2) Solar zenith angle $\theta_{\rm in} = 48^\circ$ for this paper.
3) The number of view angles n_θ was normally from one to eight, while we did some special PCA runs for n_θ up to 122.
4) The observational plane was chosen to contain the direction to the glint (azimuth angle $\Phi_{\rm out} = 0^\circ/180^\circ$) in one case (principal plane) and to be out of glint ($\Phi_{\rm out} = 48^\circ/132^\circ$) in another.
5) The number of Stokes parameters n_s was one (I: no polarization) or three (I, Q, U: linear polarization).

Fig. 2 demonstrates how the stopping rules work on the example of the model when all aerosol parameters are varied, $n_\lambda = 8$, $n_\theta = 8$, $\Phi_{\rm out} = 0^\circ/180^\circ$, and $n_s = 1$ (no polarization). The Kaiser–Guttman rules, CPV 90% and 95%, provide 5, 9, and 12 SPCs, respectively.

A. Number of SPCs: Spectral, Angular, and Polarization Information

Tables III and IV present the number of SPCs along with their respective relative contribution to the variance for all above observation situations when all aerosol parameters are varied. Tables III and IV were derived with the CPV rule 90% and 95%, respectively. In this section, we analyze the results for both cases, and in the next sections, we focus on the 90% case, which looks closer to realistic observations. Note that columns n_I and n_P in Tables III and IV contain the full number of PCs for the cases of no and linear polarizations, with which the resulting number of SPCs should be compared to estimate the information reduction.

Consider first the gradual increase in observational capabilities starting from the simplest case of one wavelength, one view angle, and no polarization. By adding more wavelength channels from one (0.533 μm) to eight (0.34–2.119 μm), we receive two to three additional SPCs that represent 93%–98% of the information. By adding more view angles from one to eight ($\theta_{\rm out} = 0^\circ - 72^\circ$), we obtain: 1) generally two to eight more SPCs; 2) three to eight more SPCs when observations are in the principal plane and two to five more SPCs when out of the plane; thus, we have one to three extra SPCs due to glint; and 3) two to seven more SPCs for the case of the fixed wind speed and two to eight more SPCs when the wind speed is varied; we anticipate that one extra SPC is due to the wind speed. As we will see below (Section III-C), the number of SPCs becomes saturated when we increase the number of view angles n_θ. By adding linear polarization (Q and U Stokes parameters), we receive: 1) one to seven further extra SPCs overall; 2) up to seven extra SPCs when observations are in the principal plane and up to six more SPCs when out of the plane; and 3) up to one extra SPC from these amounts can be related to the wind speed.

Now, we look at Tables III and IV from another view. Consider increasing the number of wavelengths in one case and the number of view angles in another case while allowing a range of wavelengths, view angles, and polarization states.

By adding more wavelength channels from one (0.533 μm) to eight (0.34–2.119 μm), we receive: 1) two to ten additional SPCs overall that represent 91%–98% of the information; 2) two to seven more SPCs when no polarization and three to ten more SPCs when linear polarization data are available; from this, we have one to three extra SPCs due to the polarization data; 3) two to ten more SPCs when observations are in the principal plane and two to eight more SPCs when out of the plane; thus, we have up to two extra SPCs from this amounts due to glint; and 4) two to seven more SPCs for the case of the fixed wind speed and two to ten more SPCs when the wind speed is varied; we expect that up to three SPCs from two to ten are associated with the wind speed.

By adding more view angles from one to eight ($\theta_{\rm out} = 0^\circ - 72^\circ$), we obtain: 1) 2–12 additional SPCs overall; 2) two to eight more SPCs when without polarization and two to ten more SPCs when with linear polarization data; we have up to four SPCs from these amounts due to the polarization data; 3) 3–12 more SPCs when observations are in the principal plane and two to seven more SPCs when out of the plane; thus, we have up to four extra SPCs due to glint; and 4) two to eight more SPCs for the case of the fixed wind speed and 2–12 more SPCs when the wind speed is varied; we anticipate that up to four extra SPCs are due to the wind speed.

As expected, Tables III and IV show a tendency of increasing the number of SPCs with an increase of any of the numbers: n_λ, n_θ, or n_s. The only exception from this rule is the transition

TABLE IV

NUMBER OF SPCS: SPECTRAL DEPENDENCE. THE RESULTS HAVE BEEN DERIVED WITH THE CPV RULE WITH THE CRITICAL CPV = 95%. n_θ IS THE NUMBER OF VIEWING DIRECTIONS COVERING $\theta_{\rm out} = 0^\circ - 72^\circ$. n_λ IS THE NUMBER OF WAVELENGTH BANDS. λ REFLECTS THE RANGE OF WAVELENGTHS. n_I (n_P) IS THE NUMBER OF PCS FOR THE CASE OF NO POLARIZATION (LINEAR POLARIZATION: THREE STOKES COMPONENTS). $n_{\rm PC}$ IS THE NUMBER OF SPCS. $\nu = 6$ m $\cdot$ s^{-1} ($\nu = 2-8$ m $\cdot$ s^{-1}) MARKS THE CASE WITH FIXED (VARIED) WIND SPEED. I (P) MARKS THE CASE OF NO (LINEAR) POLARIZATION. GL MARKS THE CASE WHEN ONE VIEWING DIRECTION IS IN GLINT: $\Phi_{\rm out} = 0^\circ/180^\circ$. OG MARKS THE CASE WHEN ALL VIEWING DIRECTIONS ARE OFF GLINT: $\Phi_{\rm out} = 48^\circ/132^\circ$. THE SOLAR ZENITH ANGLE FOR ALL THE CASES IS 48°. A SUBSCRIPT AFTER THE NUMBER OF SPCS IS THE RELATIVE CONTRIBUTION TO THE VARIANCE

n_θ	n_λ	λ (μm)	$n_{\rm I}$	$n_{\rm P}$	$n_{\rm PC}$							
					v = 6 m s^{-1}				v = 2 - 8 m s^{-1}			
					GL		OG		GL		OG	
					I	P	I	P	I	P	I	P
	1	0.533	1	3	$1_{1.00}$	$2_{0.95}$	$1_{1.00}$	$2_{0.97}$	$1_{1.00}$	$2_{0.97}$	$1_{1.00}$	$2_{0.97}$
	2	0.533 - 0.644	2	6	$2_{1.00}$	$3_{0.95}$	$2_{1.00}$	$3_{0.95}$	$2_{1.00}$	$3_{0.95}$	$2_{1.00}$	$3_{0.95}$
	3	0.533 - 0.855	3	9	$2_{0.97}$	$4_{0.96}$	$2_{0.98}$	$4_{0.96}$	$2_{0.99}$	$4_{0.97}$	$2_{0.98}$	$4_{0.96}$
1	4	0.411 - 0.855	4	12	$3_{0.99}$	$5_{0.96}$	$3_{0.99}$	$5_{0.96}$	$3_{0.99}$	$5_{0.97}$	$3_{0.99}$	$5_{0.96}$
	6	0.533 - 2.119	6	18	$3_{0.97}$	$5_{0.96}$	$3_{0.98}$	$6_{0.96}$	$3_{0.98}$	$5_{0.96}$	$3_{0.98}$	$6_{0.96}$
	7	0.411 - 2.119	7	21	$3_{0.95}$	$6_{0.96}$	$3_{0.96}$	$7_{0.96}$	$3_{0.96}$	$6_{0.96}$	$3_{0.97}$	$7_{0.96}$
	8	0.340 - 2.119	8	24	$4_{0.97}$	$7_{0.96}$	$4_{0.98}$	$8_{0.96}$	$4_{0.98}$	$7_{0.96}$	$4_{0.98}$	$8_{0.96}$
	1	0.533	2	6	$2_{1.00}$	$4_{0.96}$	$2_{1.00}$	$3_{0.95}$	$2_{1.00}$	$5_{0.99}$	$2_{1.00}$	$4_{0.98}$
	2	0.533 - 0.644	4	12	$3_{0.98}$	$5_{0.95}$	$3_{0.99}$	$4_{0.95}$	$3_{0.98}$	$5_{0.95}$	$3_{0.99}$	$5_{0.97}$
	3	0.533 - 0.855	6	18	$3_{0.96}$	$6_{0.95}$	$3_{0.97}$	$5_{0.95}$	$3_{0.96}$	$6_{0.95}$	$3_{0.97}$	$5_{0.95}$
2	4	0.411 - 0.855	8	24	$4_{0.96}$	$8_{0.95}$	$4_{0.97}$	$7_{0.96}$	$4_{0.96}$	$9_{0.96}$	$4_{0.97}$	$7_{0.96}$
	6	0.533 - 2.119	12	36	$4_{0.95}$	$7_{0.95}$	$4_{0.97}$	$7_{0.96}$	$5_{0.97}$	$8_{0.95}$	$4_{0.97}$	$7_{0.96}$
	7	0.411 - 2.119	14	42	$6_{0.97}$	$9_{0.95}$	$5_{0.97}$	$8_{0.96}$	$6_{0.97}$	$10_{0.95}$	$5_{0.97}$	$8_{0.95}$
	8	0.340 - 2.119	16	48	$7_{0.97}$	$10_{0.95}$	$5_{0.96}$	$9_{0.96}$	$7_{0.97}$	$11_{0.95}$	$5_{0.96}$	$9_{0.95}$
	1	0.533	4	12	$3_{0.97}$	$7_{0.97}$	$2_{0.97}$	$4_{0.95}$	$4_{1.00}$	$7_{0.96}$	$3_{0.98}$	$5_{0.96}$
	2	0.533 - 0.644	8	24	$4_{0.96}$	$8_{0.96}$	$3_{0.97}$	$6_{0.96}$	$5_{0.97}$	$9_{0.95}$	$4_{0.98}$	$7_{0.96}$
	3	0.533 - 0.855	12	36	$5_{0.97}$	$9_{0.96}$	$3_{0.96}$	$6_{0.95}$	$6_{0.97}$	$10_{0.95}$	$4_{0.96}$	$7_{0.95}$
4	4	0.411 - 0.855	16	48	$6_{0.95}$	$10_{0.95}$	$4_{0.97}$	$8_{0.95}$	$7_{0.96}$	$12_{0.95}$	$5_{0.96}$	$10_{0.96}$
	6	0.533 - 2.119	24	72	$6_{0.97}$	$9_{0.96}$	$4_{0.96}$	$7_{0.96}$	$7_{0.96}$	$11_{0.95}$	$5_{0.96}$	$9_{0.96}$
	7	0.411 - 2.119	28	84	$7_{0.96}$	$11_{0.95}$	$5_{0.95}$	$9_{0.95}$	$8_{0.95}$	$13_{0.95}$	$6_{0.96}$	$11_{0.95}$
	8	0.340 - 2.119	32	96	$8_{0.95}$	$13_{0.96}$	$5_{0.95}$	$10_{0.95}$	$9_{0.95}$	$15_{0.95}$	$6_{0.95}$	$12_{0.95}$
	1	0.533	8	24	$4_{0.95}$	$8_{0.95}$	$4_{0.97}$	$6_{0.95}$	$5_{0.96}$	$9_{0.95}$	$4_{0.95}$	$7_{0.95}$
	2	0.533 - 0.644	16	48	$6_{0.96}$	$9_{0.95}$	$4_{0.95}$	$7_{0.95}$	$7_{0.96}$	$11_{0.95}$	$5_{0.95}$	$8_{0.95}$
	3	0.533 - 0.855	24	72	$6_{0.96}$	$10_{0.96}$	$5_{0.95}$	$8_{0.95}$	$8_{0.96}$	$12_{0.95}$	$6_{0.95}$	$9_{0.95}$
8	4	0.411 - 0.855	32	96	$8_{0.95}$	$12_{0.95}$	$6_{0.95}$	$11_{0.95}$	$9_{0.95}$	$14_{0.95}$	$7_{0.95}$	$12_{0.95}$
	6	0.533 - 2.119	48	144	$8_{0.96}$	$11_{0.96}$	$6_{0.96}$	$9_{0.96}$	$9_{0.95}$	$13_{0.95}$	$7_{0.95}$	$10_{0.95}$
	7	0.411 - 2.119	56	168	$10_{0.95}$	$13_{0.95}$	$7_{0.95}$	$11_{0.95}$	$11_{0.95}$	$16_{0.95}$	$8_{0.95}$	$13_{0.95}$
	8	0.340 - 2.119	64	192	$11_{0.96}$	$15_{0.95}$	$8_{0.96}$	$13_{0.95}$	$12_{0.95}$	$19_{0.95}$	$9_{0.95}$	$15_{0.95}$

from the four-wavelength case (0.411–0.855 μm) to the six-wavelength (0.533–2.119 μm) when we observe occasional drops in the number of SPCs. But, this is the only transition when we not only add new channels (1.243–2.119 μm) but also remove one channel (0.411 μm). Thus, the drop indicates that the channel 0.411 μm contains more information than the three infrared channels totally.

From Tables III and IV, we can get the following estimates of SPCs for contemporary satellite instruments.

1) For the AVHRR with two submicrometer spectral channels and no polarization, we have two SPCs.
2) For the MODIS with single view direction and no polarization for the 0.53–2.1-μm spectral range, the number of SPCs is two to three.
3) For the MISR with seven view directions and no polarization for 0.53–0.86 μm, off glint, we receive three to five SPCs.
4) For the POLDER with eight simulated view directions with polarization for 0.53–0.86 μm, off glint, the number of SPCs is five to eight.
5) For the APS with eight simulated view directions and with polarization for 0.53–2.1 μm, we obtain six to nine SPCs for the off-glint observations and 7–11 SPCs for the observations in the principal plane. Note that, since the actual number of view angles for APS is significantly greater than eight (> 100), we expect a larger number of SPCs in this case (see also Section III-C).

B. Number of SPCs: Information in Single Parameters

Table VII presents the number of significant SPCs for the observation situations with one view angle $(n_\theta = 1)$ when any single aerosol parameter is fixed and the rest are varied. Table VIII is the same as Table VII except for eight view angles $(n_\theta = 8)$. The following fixed values of the parameters were used to produce the tables: $H = 1$–2 km, $\omega_o = 0.95$, $\tau = 0.2$, $\nu = 6$ km $\cdot$ s^{-1}, fine mode #2, and coarse mode #8. The results for other fixed values do not differ essentially from those in the tables.

By comparing the entry with a specific fixed parameter, with the respective entry for the case when all parameters are varied (line "All Models"), we can judge how many SPCs can be associated with the fixed parameter. We define the difference of the number of SPCs for a fixed-parameter p_i and all-varied (AM) models as: $\Delta n_{\rm SPC}(P_i) = n_{\rm SPC}({\rm AM}) - n_{\rm SPC}(P_i)$. Actually, $\Delta n_{\rm SPC}(p_i)$ is the number of SPCs associated with the fixed parameter p_i. In order to get a deeper insight into the

TABLE V
NUMBER OF SPCS ASSOCIATED WITH SINGLE PARAMETERS. CPV RULE WITH THE CRITICAL CPV = 90%. n_θ, THE NUMBER OF VIEW ANGLES, IS EQUAL TO ONE FOR ALL THE CASES: $\theta_{\rm out} = 0^\circ - 72^\circ$. n_λ IS THE NUMBER OF WAVELENGTH BANDS. λ REFLECTS THE RANGE OF WAVELENGTHS. $\nu = 6\ {\rm m \cdot s^{-1}}$ ($\nu = 2 - 8\ {\rm m \cdot s^{-1}}$) MARKS THE CASE WITH FIXED (VARIED) WIND SPEED. I (P) MARKS THE CASE OF NO (LINEAR) POLARIZATION. GL MARKS THE CASE WHEN THE VIEWING DIRECTION IS IN GLINT: $\Phi_{\rm out} = 0^\circ/180^\circ$. OG MARKS THE CASE WHEN THE VIEWING DIRECTION IS OFF GLINT: $\Phi_{\rm out} = 48^\circ/132^\circ$. THE SOLAR ZENITH ANGLE FOR ALL THE CASES IS 48°. THE RESULTS ARE PRESENTED FOR THE FOLLOWING SINGLE VARIED PARAMETERS: AEROSOL LAYER HEIGHT H, SSA OF AEROSOL PARTICLES ω_o, OPTICAL THICKNESS OF AEROSOL LAYER τ, AEROSOL MODEL, AND WIND SPEED ν. THE SUM OF THE NUMBER OF SPCS OVER ALL THE SINGLE PARAMETERS FOR EACH COLUMN IS DENOTED AS $\sum \Delta n_{\rm SPC}(P_i)$. THIS SHOULD BE COMPARED WITH THE NUMBER OF SPCS FOR THE CASE WHEN ALL SINGLE PARAMETERS ARE VARIED: LINE "ALL MODELS"

n_λ	λ (μm)	Parameters	$\Delta n_{\rm SPC}(p_i) = n_{\rm SPC}({\rm AM}) - n_{\rm SPC}(p_i)$ v = 6 m s^{-1} GL I	GL P	OG I	OG P	v = 2 - 8 m s^{-1} GL I	GL P	OG I	OG P
		H (1-2 km)	0	0	0	0	0	0	0	0
		ω_o (0.95)	0	0	0	0	0	0	0	0
		τ (0.2)	0	0	0	0	0	0	0	0
3	0.533 - 0.855	Model (#2)	0	1	1	1	0	0	1	1
		v					0	0	0	0
		$\Sigma\, \Delta n_{\rm SPC}(p_i)$	*0*	*1*	*1*	*1*	*0*	*0*	*1*	*1*
		All Models	**2**	**3**	**2**	**3**	**2**	**3**	**2**	**3**
		H (1-2 km)	0	0	0	1	0	0	0	1
		ω_o (0.95)	0	1	0	1	0	1	0	1
		τ (0.2)	0	1	0	1	0	1	0	1
4	0.411 - 0.855	Model (#2)	0	2	1	2	0	2	0	1
		v					0	0	0	0
		$\Sigma\, \Delta n_{\rm SPC}(p_i)$	*0*	*4*	*1*	*5*	*0*	*4*	*0*	*4*
		All Models	**2**	**4**	**2**	**4**	**2**	**4**	**2**	**4**
		H (1-2 km)	0	1	0	0	0	0	0	0
		ω_o (0.95)	0	1	0	1	0	1	0	0
		τ (0.2)	0	1	0	1	0	0	0	1
6	0.533 - 2.119	Model (#2)	0	2	1	2	0	1	0	2
		v					0	0	0	0
		$\Sigma\, \Delta n_{\rm SPC}(p_i)$	*0*	*5*	*1*	*4*	*0*	*2*	*0*	*3*
		All Models	**2**	**4**	**2**	**4**	**2**	**4**	**2**	**4**
		H (1-2 km)	0	0	0	1	0	0	0	0
		ω_o (0.95)	0	1	0	1	0	0	0	1
		τ (0.2)	0	1	0	1	0	0	0	1
7	0.411 - 2.119	Model (#2)	0	2	0	2	0	1	0	2
		v					0	0	0	0
		$\Sigma\, \Delta n_{\rm SPC}(p_i)$	*0*	*4*	*0*	*5*	*0*	*1*	*0*	*4*
		All Models	**2**	**4**	**2**	**5**	**2**	**4**	**2**	**5**
		H (1-2 km)	0	1	0	1	0	0	0	1
		ω_o (0.95)	0	1	1	2	0	1	0	1
		τ (0.2)	0	1	0	2	0	0	0	1
8	0.340 - 2.119	Model (#2)	1	2	1	3	0	1	1	3
		v					0	0	0	0
		$\Sigma\, \Delta n_{\rm SPC}(p_i)$	*1*	*5*	*2*	*8*	*0*	*2*	*1*	*6*
		All Models	**3**	**5**	**3**	**6**	**3**	**5**	**3**	**6**

TABLE VI
NUMBER OF SPCS ASSOCIATED WITH SINGLE PARAMETERS. CPV RULE WITH THE CRITICAL CPV = 90%. n_θ, THE NUMBER OF VIEW ANGLES, IS EQUAL TO EIGHT FOR ALL THE CASES: $\theta_{\rm out} = 0^\circ - 72^\circ$. n_λ IS THE NUMBER OF WAVELENGTH BANDS. λ REFLECTS THE RANGE OF WAVELENGTHS. $\nu = 6\ {\rm m \cdot s^{-1}}$ ($\nu = 2 - 8\ {\rm m \cdot s^{-1}}$) MARKS THE CASE WITH FIXED (VARIED) WIND SPEED. I (P) MARKS THE CASE OF NO (LINEAR) POLARIZATION. GL MARKS THE CASE WHEN THE VIEWING DIRECTION IS IN GLINT: $\Phi_{\rm out} = 0^\circ/180^\circ$. OG MARKS THE CASE WHEN THE VIEWING DIRECTION IS OFF GLINT: $\Phi_{\rm out} = 48^\circ/132^\circ$. THE SOLAR ZENITH ANGLE FOR ALL THE CASES IS 48°. THE RESULTS ARE PRESENTED FOR THE FOLLOWING SINGLE VARIED PARAMETERS: AEROSOL LAYER HEIGHT H, SSA OF AEROSOL PARTICLES ω_o, OPTICAL THICKNESS OF AEROSOL LAYER τ, AEROSOL MODEL, AND WIND SPEED ν. THE SUM OF THE NUMBER OF SPCS OVER ALL THE SINGLE PARAMETERS FOR EACH COLUMN IS DENOTED AS $\sum \Delta n_{\rm SPC}(p_i)$. THIS SHOULD BE COMPARED WITH THE NUMBER OF SPCS FOR THE CASE WHEN ALL SINGLE PARAMETERS ARE VARIED: LINE "ALL MODELS"

n_λ	λ (μm)	Parameters	$\Delta n_{\rm SPC}(p_i) = n_{\rm SPC}({\rm AM}) - n_{\rm SPC}(p_i)$ v = 6 m s^{-1} GL I	GL P	OG I	OG P	v = 2 - 8 m s^{-1} GL I	GL P	OG I	OG P
		H (1-2 km)	0	1	0	1	0	2	0	1
		ω_o (0.95)	1	1	0	1	1	2	1	1
		τ (0.2)	1	2	0	1	1	3	1	1
3	0.533 - 0.855	Model (#2)	3	4	1	2	3	4	2	2
		v					1	2	1	0
		$\Sigma\, \Delta n_{\rm SPC}(p_i)$	*5*	*8*	*1*	*5*	*6*	*13*	*5*	*5*
		All Models	**5**	**7**	**3**	**5**	**6**	**9**	**4**	**6**
		H (1-2 km)	1	2	0	1	1	1	1	1
		ω_o (0.95)	1	2	1	1	1	2	1	1
		τ (0.2)	1	3	1	2	1	2	1	2
4	0.411 - 0.855	Model (#2)	3	5	2	4	3	5	2	4
		v					1	1	1	1
		$\Sigma\, \Delta n_{\rm SPC}(p_i)$	*6*	*12*	*4*	*8*	*7*	*11*	*6*	*9*
		All Models	**6**	**9**	**4**	**7**	**7**	**10**	**5**	**8**
		H (1-2 km)	1	2	1	1	1	1	1	1
		ω_o (0.95)	1	2	1	1	1	1	1	1
		τ (0.2)	2	3	1	2	2	2	1	2
6	0.533 - 2.119	Model (#2)	3	4	2	3	3	4	3	3
		v					1	1	1	1
		$\Sigma\, \Delta n_{\rm SPC}(p_i)$	*7*	*11*	*5*	*7*	*8*	*9*	*7*	*8*
		All Models	**6**	**8**	**4**	**6**	**7**	**9**	**5**	**7**
		H (1-2 km)	1	2	1	2	1	2	1	1
		ω_o (0.95)	2	3	2	2	2	2	2	1
		τ (0.2)	2	3	2	3	2	3	2	2
7	0.411 - 2.119	Model (#2)	4	6	3	4	4	5	3	4
		v					1	1	1	1
		$\Sigma\, \Delta n_{\rm SPC}(p_i)$	*9*	*14*	*8*	*11*	*10*	*13*	*9*	*9*
		All Models	**7**	**10**	**6**	**8**	**8**	**11**	**6**	**9**
		H (1-2 km)	2	2	1	2	2	2	1	2
		ω_o (0.95)	2	3	1	2	2	3	2	3
		τ (0.2)	3	4	1	3	2	3	2	4
8	0.340 - 2.119	Model (#2)	4	6	3	5	4	5	3	5
		v					1	1	1	1
		$\Sigma\, \Delta n_{\rm SPC}(p_i)$	*11*	*15*	*6*	*12*	*11*	*14*	*9*	*15*
		All Models	**8**	**11**	**5**	**9**	**9**	**12**	**6**	**10**

problem, we compiled two more tables (Tables V and VI) which contain the differences $\Delta n_{\rm SPC}(p_i)$ for the cases of $n_\theta = 1$ and 8, respectively. The tables also contain lines with sums of the differences over all fixed parameters $\sum_i \Delta n_{\rm SPC}(p_i)$ and the number of SPCs from the all-varied models to compare with. When the sum of the differences is less than the total number of SPCs, then some of the parameters cannot be retrieved within the accuracy of the observations. On the other hand, if the sum of the differences is greater than or equal to the total number of SPCs, then there should be one or more SPCs per parameter, or some of the SPCs can be shared between different parameters, reflecting nonlinear relationships between the parameters. However, even in such cases, the information about some of the parameters, for which the difference of the numbers is zero, may not still be retrieved.

TABLE VII

NUMBER OF SPCS: INFORMATION IN SINGLE PARAMETERS. THE NUMBER OF PCS IS FIRST GIVEN TO A COMBINATION OF ALL AEROSOL MODELS, THAN FOR A FIXED PARAMETER, ONE AT A TIME. n_θ, THE NUMBER OF VIEWING DIRECTIONS, IS EQUAL TO ONE FOR ALL THE CASES: $\theta_{\rm out} = 0^\circ - 72^\circ$. n_λ IS THE NUMBER OF WAVELENGTH BANDS. λ REFLECTS THE RANGE OF WAVELENGTHS. n_I (n_P) IS THE NUMBER OF PCS FOR THE CASE OF NO POLARIZATION (LINEAR POLARIZATION: THREE STOKES PARAMETERS). $n_{\rm PC}$ IS THE NUMBER OF SPCS. $\nu = 6\ {\rm m \cdot s^{-1}}$ $(\nu = 2{-}8\ {\rm m \cdot s^{-1}})$ MARKS THE CASE WITH FIXED (VARIED) WIND SPEED. I (P) MARKS THE CASE OF NO (LINEAR) POLARIZATION. GL MARKS THE CASE WHEN THE VIEWING DIRECTION IS IN GLINT: $\Phi_{\rm out} = 0^\circ/180^\circ$. OG MARKS THE CASE WHEN THE VIEWING DIRECTION IS OFF GLINT: $\Phi_{\rm out} = 48^\circ/132^\circ$. THE SOLAR ZENITH ANGLE FOR ALL THE CASES IS 48°. A SUBSCRIPT AFTER A NUMBER OF SPCS IS THE RELATIVE CONTRIBUTION TO THE VARIANCE

n_λ	λ (μm)	$n_{\rm I}$	$n_{\rm P}$	Parameters	$n_{\rm PC}$							
					v = 6 m s^{-1}				v = 2 - 8 m s^{-1}			
					GL		OG		GL		OG	
					I	P	I	P	I	P	I	P
3	0.533 - 0.855	3	9	All Models	$2_{0.97}$	$3_{0.92}$	$2_{0.98}$	$3_{0.93}$	$2_{0.99}$	$3_{0.92}$	$2_{0.98}$	$3_{0.93}$
				Fixed H (1-2 km)	$2_{0.98}$	$3_{0.93}$	$2_{0.98}$	$3_{0.94}$	$2_{0.99}$	$3_{0.92}$	$2_{0.98}$	$3_{0.94}$
				Fixed ω_0 (0.95)	$2_{0.97}$	$3_{0.95}$	$2_{0.98}$	$3_{0.96}$	$2_{0.99}$	$3_{0.93}$	$2_{0.98}$	$3_{0.97}$
				Fixed τ (0.2)	$2_{0.98}$	$3_{0.94}$	$2_{0.98}$	$3_{0.96}$	$2_{0.99}$	$3_{0.91}$	$2_{0.98}$	$3_{0.95}$
				Fine Particles	$2_{0.97}$	$3_{0.94}$	$2_{0.98}$	$3_{0.95}$	$2_{0.99}$	$3_{0.94}$	$2_{0.99}$	$3_{0.94}$
				Coarse Particles	$1_{0.98}$	$2_{0.98}$	$1_{0.98}$	$2_{0.90}$	$1_{0.99}$	$2_{0.98}$	$1_{0.98}$	$2_{0.90}$
				1 Fine Mode (#2)	$2_{0.99}$	$2_{0.96}$	$1_{0.91}$	$2_{0.92}$	$2_{0.99}$	$2_{0.94}$	$1_{0.91}$	$2_{0.91}$
				1 Coarse Mode (#8)	$1_{0.98}$	$1_{0.93}$	$1_{0.99}$	$2_{0.90}$	$1_{0.99}$	$2_{0.99}$	$1_{0.99}$	$2_{0.90}$
4	0.411 - 0.855	4	12	All Models	$2_{0.90}$	$4_{0.93}$	$2_{0.94}$	$4_{0.92}$	$2_{0.94}$	$4_{0.94}$	$2_{0.94}$	$4_{0.91}$
				Fixed H (1-2 km)	$2_{0.90}$	$4_{0.94}$	$2_{0.98}$	$3_{0.94}$	$2_{0.95}$	$4_{0.95}$	$2_{0.94}$	$3_{0.90}$
				Fixed ω_0 (0.95)	$2_{0.90}$	$3_{0.93}$	$2_{0.98}$	$3_{0.96}$	$2_{0.95}$	$3_{0.91}$	$2_{0.97}$	$3_{0.91}$
				Fixed τ (0.2)	$2_{0.91}$	$3_{0.90}$	$2_{0.98}$	$3_{0.96}$	$2_{0.97}$	$3_{0.90}$	$2_{0.94}$	$3_{0.90}$
				Fine Particles	$2_{0.90}$	$3_{0.91}$	$2_{0.99}$	$3_{0.95}$	$2_{0.95}$	$3_{0.90}$	$2_{0.96}$	$3_{0.90}$
				Coarse Particles	$2_{0.98}$	$2_{0.92}$	$1_{0.98}$	$2_{0.90}$	$2_{0.99}$	$2_{0.96}$	$2_{0.99}$	$3_{0.90}$
				1 Fine Mode (#2)	$2_{0.97}$	$2_{0.93}$	$1_{0.99}$	$2_{0.90}$	$2_{0.98}$	$2_{0.90}$	$2_{0.99}$	$3_{0.94}$
				1 Coarse Mode (#8)	$2_{0.97}$	$2_{0.93}$	$1_{0.99}$	$2_{0.90}$	$2_{0.99}$	$2_{0.96}$	$2_{0.99}$	$3_{0.90}$
6	0.533 - 2.119	6	18	All Models	$2_{0.92}$	$4_{0.93}$	$2_{0.93}$	$4_{0.91}$	$2_{0.94}$	$4_{0.93}$	$2_{0.93}$	$4_{0.91}$
				Fixed H (1-2 km)	$2_{0.93}$	$3_{0.90}$	$2_{0.93}$	$4_{0.92}$	$2_{0.94}$	$4_{0.93}$	$2_{0.93}$	$4_{0.91}$
				Fixed ω_0 (0.95)	$2_{0.94}$	$3_{0.92}$	$2_{0.93}$	$3_{0.90}$	$2_{0.95}$	$3_{0.90}$	$2_{0.94}$	$4_{0.93}$
				Fixed τ (0.2)	$2_{0.94}$	$3_{0.93}$	$2_{0.95}$	$3_{0.92}$	$2_{0.95}$	$4_{0.93}$	$2_{0.94}$	$3_{0.90}$
				Fine Particles	$2_{0.90}$	$3_{0.90}$	$2_{0.93}$	$3_{0.91}$	$2_{0.92}$	$4_{0.92}$	$2_{0.94}$	$3_{0.90}$
				Coarse Particles	$1_{0.92}$	$2_{0.96}$	$1_{0.96}$	$2_{0.90}$	$1_{0.97}$	$2_{0.97}$	$1_{0.97}$	$3_{0.90}$
				1 Fine Mode (#2)	$2_{0.92}$	$2_{0.93}$	$1_{0.90}$	$2_{0.93}$	$2_{0.94}$	$3_{0.93}$	$2_{0.98}$	$2_{0.92}$
				1 Coarse Mode (#8)	$1_{0.94}$	$1_{0.91}$	$1_{0.99}$	$2_{0.90}$	$1_{0.97}$	$2_{0.98}$	$1_{0.99}$	$3_{0.94}$
7	0.411 - 2.119	7	21	All Models	$2_{0.90}$	$4_{0.91}$	$2_{0.90}$	$5_{0.90}$	$2_{0.91}$	$4_{0.90}$	$2_{0.90}$	$5_{0.90}$
				Fixed H (1-2 km)	$2_{0.90}$	$4_{0.92}$	$2_{0.90}$	$4_{0.90}$	$2_{0.92}$	$4_{0.91}$	$2_{0.90}$	$5_{0.91}$
				Fixed ω_0 (0.95)	$2_{0.90}$	$3_{0.90}$	$2_{0.92}$	$4_{0.92}$	$2_{0.92}$	$4_{0.93}$	$2_{0.92}$	$4_{0.90}$
				Fixed τ (0.2)	$2_{0.90}$	$3_{0.90}$	$2_{0.92}$	$4_{0.92}$	$2_{0.93}$	$4_{0.91}$	$2_{0.91}$	$4_{0.90}$
				Fine Particles	$2_{0.90}$	$3_{0.90}$	$2_{0.90}$	$4_{0.92}$	$2_{0.90}$	$4_{0.90}$	$2_{0.91}$	$4_{0.91}$
				Coarse Particles	$2_{0.93}$	$3_{0.96}$	$2_{0.97}$	$4_{0.93}$	$2_{0.97}$	$2_{0.95}$	$2_{0.97}$	$4_{0.90}$
				1 Fine Mode (#2)	$2_{0.90}$	$2_{0.90}$	$2_{0.97}$	$3_{0.95}$	$2_{0.91}$	$3_{0.91}$	$2_{0.96}$	$3_{0.94}$
				1 Coarse Mode (#8)	$2_{0.95}$	$2_{0.91}$	$2_{0.99}$	$3_{0.93}$	$2_{0.97}$	$2_{0.96}$	$2_{0.99}$	$3_{0.90}$
8	0.340 - 2.119	8	24	All Models	$3_{0.93}$	$5_{0.92}$	$3_{0.94}$	$6_{0.92}$	$3_{0.94}$	$5_{0.91}$	$3_{0.94}$	$6_{0.92}$
				Fixed H (1-2 km)	$3_{0.93}$	$4_{0.91}$	$3_{0.94}$	$5_{0.91}$	$3_{0.95}$	$5_{0.92}$	$3_{0.94}$	$5_{0.90}$
				Fixed ω_0 (0.95)	$3_{0.95}$	$4_{0.92}$	$2_{0.90}$	$4_{0.91}$	$3_{0.95}$	$4_{0.90}$	$3_{0.97}$	$5_{0.92}$
				Fixed τ (0.2)	$3_{0.96}$	$4_{0.92}$	$3_{0.94}$	$4_{0.90}$	$3_{0.95}$	$5_{0.93}$	$3_{0.94}$	$5_{0.91}$
				Fine Particles	$3_{0.92}$	$4_{0.90}$	$2_{0.90}$	$4_{0.90}$	$3_{0.94}$	$5_{0.91}$	$3_{0.95}$	$4_{0.90}$
				Coarse Particles	$2_{0.92}$	$3_{0.92}$	$2_{0.95}$	$4_{0.90}$	$2_{0.97}$	$3_{0.95}$	$2_{0.96}$	$4_{0.90}$
				1 Fine Mode (#2)	$2_{0.90}$	$3_{0.92}$	$2_{0.96}$	$3_{0.94}$	$3_{0.97}$	$4_{0.93}$	$2_{0.96}$	$3_{0.92}$
				1 Coarse Mode (#8)	$2_{0.93}$	$3_{0.95}$	$2_{0.96}$	$3_{0.90}$	$2_{0.97}$	$2_{0.90}$	$2_{0.97}$	$4_{0.94}$

We can see the following general tendencies in Tables V and VI: 1) Most SPCs per parameter (up to three for one view angle and up to six for eight view angles) are due to aerosol model, with smaller amounts due to τ (up to two and four), ω_o (up to two and three), and H (up to one and two); 2) for the case of eight view angles, more SPCs per parameter (up to two extra) come from the in-glint observations compared with the out-of-glint observations, whereas for the case of one view angle, we observe the inverse situation: the out-of-glint observations sometimes can provide one to two extra SPCs per parameter; 3) one stable SPC, due to the wind speed, can be derived from the eight-angle observations, whereas no wind speed information is in the one-angle observations; and 4) linear polarization observations can provide up to two extra SPCs per parameter and no matter in-glint or out-of-glint and one-angle or eight-angle observations.

Table IX presents another view on the number of SPCs in single parameters, for the case of seven wavelengths and eight viewing directions. We started from the case when all parameters are varied: this is the top of the pyramid. Then, we ran the PCA for the fine and coarse modes separately. Then, for each mode, we did the PCA for a single aerosol model (#2 fine and #8 coarse). After this step, we consecutively fixed the parameters until just one parameter is allowed to vary: the results at this final step form the pyramid base. By comparing the number of SPCs between the two consecutive steps, we can estimate the number of SPCs associated with the fixed parameter.

TABLE VIII

NUMBER OF SPCs: INFORMATION IN SINGLE PARAMETERS. THE NUMBER OF PCs IS FIRST GIVEN TO A COMBINATION OF ALL AEROSOL MODELS, THAN FOR A FIXED PARAMETER, ONE AT A TIME. n_θ, THE NUMBER OF VIEWING DIRECTIONS, IS EQUAL TO EIGHT FOR ALL THE CASES: $\theta_{\rm out} = 0^\circ - 72^\circ$. n_λ IS THE NUMBER OF WAVELENGTH BANDS. λ REFLECTS THE RANGE OF WAVELENGTHS. n_I (n_P) IS THE NUMBER OF PCs FOR THE CASE OF NO POLARIZATION (LINEAR POLARIZATION: THREE STOKES PARAMETERS). $n_{\rm PC}$ IS THE NUMBER OF SPCs. $\nu = 6\ {\rm m \cdot s^{-1}}$ ($\nu = 2{-}8\ {\rm m \cdot s^{-1}}$) MARKS THE CASE WITH FIXED (VARIED) WIND SPEED. I (P) MARKS THE CASE OF NO (LINEAR) POLARIZATION. GL MARKS THE CASE WHEN ONE VIEWING DIRECTION IS IN GLINT: $\Phi_{\rm out} = 0^\circ/180^\circ$. OG MARKS THE CASE WHEN ALL VIEWING DIRECTIONS ARE OFF GLINT: $\Phi_{\rm out} = 48^\circ/132^\circ$. THE SOLAR ZENITH ANGLE FOR ALL THE CASES IS 48°. A SUBSCRIPT AFTER A NUMBER OF SPCs IS THE RELATIVE CONTRIBUTION TO THE VARIANCE

n_λ	λ (μm)	$n_{\rm I}$	$n_{\rm P}$	Parameters	$n_{\rm PC}$							
					v = 6 m s^{-1}				v = 2 - 8 m s^{-1}			
					GL		OG		GL		OG	
					I	P	I	P	I	P	I	P
3	0.533 - 0.855	24	72	All Models	$5_{0.93}$	$7_{0.91}$	$3_{0.90}$	$5_{0.90}$	$6_{0.92}$	$9_{0.91}$	$4_{0.92}$	$6_{0.90}$
				Fixed H (1-2 km)	$5_{0.94}$	$6_{0.92}$	$3_{0.92}$	$4_{0.90}$	$6_{0.93}$	$7_{0.90}$	$4_{0.93}$	$5_{0.90}$
				Fixed $\omega_{\rm o}$ (0.95)	$4_{0.90}$	$6_{0.92}$	$3_{0.94}$	$4_{0.91}$	$5_{0.92}$	$7_{0.90}$	$3_{0.90}$	$5_{0.91}$
				Fixed τ (0.2)	$4_{0.93}$	$5_{0.92}$	$3_{0.93}$	$4_{0.93}$	$5_{0.93}$	$6_{0.90}$	$3_{0.90}$	$5_{0.92}$
				Fine Particles	$3_{0.92}$	$6_{0.90}$	$3_{0.93}$	$4_{0.90}$	$4_{0.90}$	$7_{0.90}$	$4_{0.93}$	$5_{0.90}$
				Coarse Particles	$3_{0.97}$	$4_{0.95}$	$2_{0.96}$	$3_{0.92}$	$3_{0.94}$	$5_{0.95}$	$2_{0.91}$	$4_{0.91}$
				1 Fine Mode (#2)	$2_{0.90}$	$4_{0.94}$	$2_{0.95}$	$3_{0.92}$	$3_{0.92}$	$5_{0.93}$	$2_{0.91}$	$4_{0.91}$
				1 Coarse Mode (#8)	$2_{0.97}$	$3_{0.97}$	$1_{0.95}$	$2_{0.90}$	$2_{0.92}$	$3_{0.90}$	$2_{0.95}$	$3_{0.90}$
4	0.411 - 0.855	32	96	All Models	$6_{0.91}$	$9_{0.91}$	$4_{0.91}$	$7_{0.90}$	$7_{0.90}$	$10_{0.90}$	$5_{0.92}$	$8_{0.90}$
				Fixed H (1-2 km)	$5_{0.90}$	$7_{0.90}$	$4_{0.93}$	$6_{0.91}$	$6_{0.90}$	$9_{0.90}$	$4_{0.90}$	$7_{0.90}$
				Fixed $\omega_{\rm o}$ (0.95)	$5_{0.91}$	$7_{0.92}$	$3_{0.91}$	$6_{0.92}$	$6_{0.91}$	$8_{0.90}$	$4_{0.92}$	$7_{0.91}$
				Fixed τ (0.2)	$5_{0.91}$	$6_{0.90}$	$3_{0.90}$	$5_{0.91}$	$6_{0.91}$	$8_{0.91}$	$4_{0.90}$	$6_{0.90}$
				Fine Particles	$5_{0.93}$	$7_{0.91}$	$3_{0.90}$	$5_{0.90}$	$6_{0.92}$	$8_{0.90}$	$4_{0.90}$	$6_{0.90}$
				Coarse Particles	$4_{0.94}$	$5_{0.94}$	$2_{0.90}$	$4_{0.90}$	$4_{0.92}$	$6_{0.93}$	$3_{0.91}$	$6_{0.92}$
				1 Fine Mode (#2)	$3_{0.93}$	$4_{0.92}$	$2_{0.92}$	$3_{0.90}$	$4_{0.93}$	$5_{0.91}$	$3_{0.92}$	$4_{0.90}$
				1 Coarse Mode (#8)	$3_{0.94}$	$4_{0.95}$	$2_{0.93}$	$3_{0.90}$	$3_{0.91}$	$5_{0.94}$	$2_{0.90}$	$4_{0.90}$
6	0.533 - 2.119	48	144	All Models	$6_{0.93}$	$8_{0.92}$	$4_{0.92}$	$6_{0.92}$	$7_{0.92}$	$9_{0.90}$	$5_{0.92}$	$7_{0.91}$
				Fixed H (1-2 km)	$5_{0.91}$	$6_{0.91}$	$3_{0.90}$	$5_{0.90}$	$6_{0.90}$	$8_{0.90}$	$4_{0.90}$	$6_{0.90}$
				Fixed $\omega_{\rm o}$ (0.95)	$5_{0.92}$	$6_{0.92}$	$3_{0.92}$	$5_{0.93}$	$6_{0.92}$	$8_{0.91}$	$4_{0.91}$	$6_{0.91}$
				Fixed τ (0.2)	$4_{0.92}$	$5_{0.91}$	$3_{0.92}$	$4_{0.92}$	$5_{0.91}$	$7_{0.91}$	$4_{0.91}$	$5_{0.90}$
				Fine Particles	$4_{0.90}$	$6_{0.90}$	$3_{0.90}$	$5_{0.91}$	$5_{0.90}$	$7_{0.90}$	$4_{0.90}$	$6_{0.90}$
				Coarse Particles	$3_{0.97}$	$3_{0.91}$	$2_{0.95}$	$3_{0.90}$	$3_{0.92}$	$4_{0.90}$	$3_{0.94}$	$4_{0.90}$
				1 Fine Mode (#2)	$3_{0.93}$	$4_{0.92}$	$2_{0.95}$	$3_{0.90}$	$4_{0.92}$	$5_{0.90}$	$2_{0.91}$	$4_{0.90}$
				1 Coarse Mode (#8)	$2_{0.97}$	$2_{0.91}$	$1_{0.95}$	$2_{0.90}$	$2_{0.92}$	$3_{0.90}$	$2_{0.95}$	$3_{0.90}$
7	0.411 - 2.119	56	168	All Models	$7_{0.91}$	$10_{0.92}$	$5_{0.92}$	$8_{0.90}$	$8_{0.91}$	$11_{0.90}$	$6_{0.92}$	$9_{0.90}$
				Fixed H (1-2 km)	$6_{0.90}$	$8_{0.92}$	$4_{0.92}$	$6_{0.90}$	$7_{0.90}$	$9_{0.90}$	$5_{0.91}$	$8_{0.90}$
				Fixed $\omega_{\rm o}$ (0.95)	$5_{0.90}$	$7_{0.91}$	$3_{0.90}$	$6_{0.90}$	$6_{0.90}$	$9_{0.91}$	$4_{0.90}$	$8_{0.91}$
				Fixed τ (0.2)	$5_{0.91}$	$7_{0.93}$	$3_{0.91}$	$5_{0.91}$	$6_{0.90}$	$8_{0.90}$	$4_{0.90}$	$7_{0.91}$
				Fine Particles	$5_{0.90}$	$7_{0.90}$	$4_{0.92}$	$6_{0.90}$	$6_{0.90}$	$9_{0.90}$	$5_{0.91}$	$7_{0.90}$
				Coarse Particles	$4_{0.95}$	$5_{0.94}$	$3_{0.94}$	$5_{0.93}$	$4_{0.91}$	$6_{0.93}$	$4_{0.93}$	$6_{0.92}$
				1 Fine Mode (#2)	$3_{0.90}$	$4_{0.91}$	$2_{0.92}$	$4_{0.94}$	$4_{0.90}$	$6_{0.91}$	$3_{0.92}$	$5_{0.93}$
				1 Coarse Mode (#8)	$3_{0.95}$	$4_{0.96}$	$2_{0.93}$	$4_{0.94}$	$3_{0.91}$	$5_{0.94}$	$3_{0.93}$	$5_{0.93}$
8	0.340 - 2.119	64	192	All Models	$8_{0.92}$	$11_{0.91}$	$5_{0.91}$	$9_{0.91}$	$9_{0.92}$	$12_{0.90}$	$6_{0.91}$	$10_{0.90}$
				Fixed H (1-2 km)	$6_{0.91}$	$9_{0.92}$	$4_{0.91}$	$7_{0.91}$	$7_{0.90}$	$10_{0.90}$	$5_{0.91}$	$9_{0.91}$
				Fixed $\omega_{\rm o}$ (0.95)	$6_{0.92}$	$8_{0.92}$	$4_{0.92}$	$7_{0.92}$	$7_{0.91}$	$9_{0.90}$	$4_{0.90}$	$8_{0.90}$
				Fixed τ (0.2)	$5_{0.90}$	$7_{0.91}$	$4_{0.91}$	$6_{0.92}$	$7_{0.92}$	$9_{0.91}$	$4_{0.90}$	$7_{0.90}$
				Fine Particles	$6_{0.91}$	$8_{0.90}$	$4_{0.90}$	$7_{0.91}$	$7_{0.90}$	$10_{0.90}$	$5_{0.90}$	$8_{0.90}$
				Coarse Particles	$4_{0.92}$	$5_{0.92}$	$3_{0.92}$	$5_{0.91}$	$5_{0.93}$	$6_{0.91}$	$4_{0.92}$	$6_{0.91}$
				1 Fine Mode (#2)	$4_{0.93}$	$5_{0.93}$	$2_{0.91}$	$4_{0.93}$	$5_{0.92}$	$7_{0.92}$	$3_{0.91}$	$5_{0.92}$
				1 Coarse Mode (#8)	$3_{0.92}$	$4_{0.93}$	$2_{0.92}$	$4_{0.92}$	$3_{0.90}$	$5_{0.92}$	$3_{0.92}$	$5_{0.92}$

After analyzing the results reported in Tables V–IX, we can conclude that, generally, observations are most sensitive to aerosol model, followed in decreasing order by τ, $\omega_{\rm o}$, and H. The sensitivity to the wind speed ν depends on the number of view angles. Because each of the aerosol models used by us already incorporates specific values of the size distribution parameters and refractive index, it is impossible to further estimate how many SPCs from those associated with the aerosol model can be related with the size distribution parameters and with the refractive index. Thus, for example, the impact of the refractive index cannot be estimated here. To achieve it, a PCA should be done with both the refractive index and the size distribution parameters as directly varied parameters. Note that Mishchenko and Travis [18]–[20] performed the sensitivity study by varying both the refractive index and the size distribution for single-wavelength measurements.

C. Number of SPCs Versus the Position of the Observational Plane

Figs. 3 and 4 display the plots of the number of SPCs as a function of the number of view angles and the azimuth angle of the observational plane. The results are presented for three sets of wavelength bands $(n_\lambda = 4, 7, \text{and}, 8)$, for observations without and with linear polarizations and for the cases when the wind speed is varied and fixed.

The figures demonstrate that there is a saturation effect when we increase the number of view angles n_θ: no

TABLE IX

NUMBER OF SPCS: VARIED AND FIXED PARAMETERS, SEVEN WAVELENGTHS, AND EIGHT VIEWING DIRECTIONS. THE SOLAR ZENITH ANGLE FOR ALL THE CASES IS 48°, AND THE NUMBER OF VIEWING DIRECTIONS n_θ IS EIGHT. THE LEFT NUMBER CORRESPONDS TO THE CASE WHEN THE VIEWING DIRECTIONS LIE IN THE PRINCIPAL PLANE: $\theta_{\rm out} = 0°-72°$ AND $\Phi_{\rm out} = 0°/180°$, THUS CONTAINING THE DIRECTION TO THE GLINT CENTER. THE RIGHT NUMBER CORRESPONDS TO THE VIEWING DIRECTIONS IN ANOTHER PLANE LOCATED OUT OF THE GLINT: $\theta_{\rm out} = 0°-72°$ AND $\Phi_{\rm out} = 48°/132°$. VARIED AND FIXED PARAMETERS ARE AEROSOL MODEL, WIND SPEED (MARKED AS W), AEROSOL LAYER HEIGHT (H), AEROSOL SSA (A), AND AOT (T). FIXED PARAMETERS ARE SUBSCRIPTED e.g., (WHAT). THE CASES WHEN THE PROGRAM FAILED TO FIND THE PCS ARE MARKED BY "-"

Varied Wind Speed (2-8 m s^{-1})																			
No Polarization (1 Stokes Parameter: *I*)																			
All Models																			
8 • 6																			
Fine Mode												Coarse Mode							
6 • 5												4 • 4							
Fixed Fine Model (#2): WHAT												Fixed Coarse Model (#8): WHAT							
4 • 3												3 • 3							
WHA_T		WH_AT		W_HAT		$_WHAT$				WHA_T		WH_AT		W_HAT		$_WHAT$			
3 • 3		3 • 2		3 • 2		3 • 2				3 • 3		2 • 2		3 • 2		3 • 2			
WH_AT	W_HA_T	W_HAT	$_WHA_T$	$_WH_AT$	$_WHAT$					WH_AT	W_HA_T	W_HAT	$_WHA_T$	$_WH_AT$	$_WHAT$				
- • -	3 • 2	2 • 1	2 • 2	2 • 1	2 • 2					2 • 2	- • -	2 • 1	2 • 2	2 • 1	3 • 2				
W_HAT		$_WH_AT$		$_WHA_T$		$_WHAT$				W_HAT		$_WH_AT$		$_WHA_T$		$_WHAT$			
- • -		- • -		1 • 1		2 • 1				- • -		1 • 1		- • -		2 • 1			
Linear Polarization (3 Stokes Parameters: *I*, *Q*, *U*)																			
All Models																			
11 • 9																			
Fine Mode												Coarse Mode							
9 • 7												6 • 6							
Fixed Fine Model (#2): WHAT												Fixed Coarse Model (#8): WHAT							
6 • 5												5 • 5							
WHA_T		WH_AT		W_HAT		$_WHAT$				WHA_T		WH_AT		W_HAT		$_WHAT$			
5 • 4		4 • 3		4 • 4		4 • 4				4 • 3		4 • 4		4 • 4		4 • 4			
WH_AT	W_HA_T	W_HAT	$_WHA_T$	$_WH_AT$	$_WHAT$					WH_AT	W_HA_T	W_HAT	$_WHA_T$	$_WH_AT$	$_WHAT$				
- • -	3 • 3	3 • 2	3 • 3	3 • 2	3 • 3					3 • 2	- • -	3 • 3	3 • 2	3 • 3	3 • 3				
W_HAT		$_WH_AT$		$_WHA_T$		$_WHAT$				W_HAT		$_WH_AT$		$_WHA_T$		$_WHAT$			
- • -		- • -		2 • 2		2 • 2				- • -		2 • 2		- • -		2 • 2			
Fixed Wind Speed (6 m s^{-1})																			
No Polarization (1 Stokes Parameter: *I*)																			
All Models																			
7 • 5																			
Fine Mode												Coarse Mode							
5 • 4												4 • 3							
Fixed Fine Model (#2): HAT												Fixed Coarse Model (#8): HAT							
3 • 2												3 • 2							
HA_T		H_AT		$_HAT$						HA_T		H_AT		$_HAT$					
2 • 2		2 • 1		2 • 2						2 • 2		2 • 1		3 • 2					
H_AT		$_HA_T$		$_HAT$						H_AT		$_HA_T$		$_HAT$					
- • -		1 • 1		2 • 1						1 • 1		- • -		2 • 1					
Linear Polarization (3 Stokes Parameters: *I*, *Q*, *U*)																			
All Models																			
10 • 8																			
Fine Mode												Coarse Mode							
7 • 6												5 • 5							
Fixed Fine Model (#2): $_WHAT$												Fixed Coarse Model (#8): $_WHAT$							
4 • 4												4 • 4							
HA_T		H_AT		$_HAT$						HA_T		H_AT		$_HAT$					
3 • 3		3 • 2		3 • 3						3 • 2		3 • 3		3 • 3					
H_AT		$_HA_T$		$_HAT$						H_AT		$_HA_T$		$_HAT$					
- • -		2 • 2		2 • 2						2 • 2		- • -		2 • 2					

significant change in the number of SPCs for $n_\theta \geq 10-15$ when no polarization and for $n_\theta \geq 30$ with linear polarization data. The saturation appears because we increase the number of view angles $\theta_{\rm out}$, but keep them in the range $1.5° \leq \theta_{\rm out} \leq 72°$. Thus, starting from some point, no new information is added.

Depending on the position of the observational plane, we can get from two to ten SPCs without polarization and from 4 to 16 SPCs with linear polarization data. Up to two SPCs should be due to the wind speed. Observations with seven and eight wavelength bands can provide one to three more SPCs compared with the case of four bands.

When moving the observation plane from $\Phi_{\rm out} = 0°/180°$ to $90°/90°$, there is a general drop in the number of SPCs, which reflects a drop in the information content due to narrowing the range of scattering angles from $0°-120°$ to $48°-78°$.

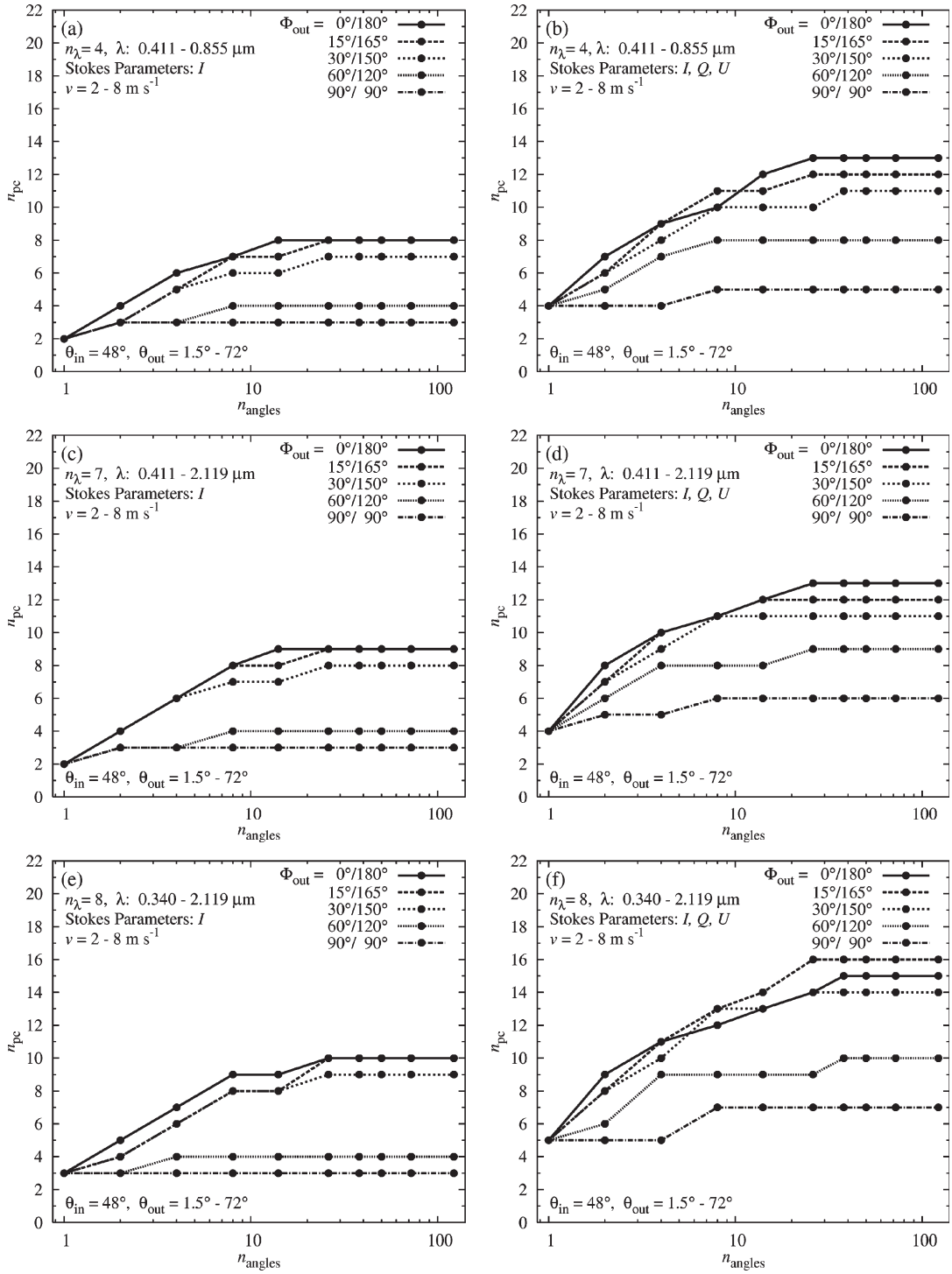

Fig. 3. Number of SPCs as a function of the number of viewing directions for $\theta_{\rm in} = 48^\circ$, $\theta_{\rm out} = 1.5^\circ - 72^\circ$, and $\Phi_{\rm out} = 0^\circ/180^\circ - 90^\circ/90^\circ$, and with the wind speed varied in the range of 2–8 m $\cdot$ s^{-1} for (a) four wavelength bands (0.411–0.855 μm) and no polarization, (b) four wavelength bands (0.411–0.855 μm) and with linear polarization, (c) seven wavelength bands (0.411–2.119 μm) and no polarization, (d) seven wavelength bands (0.411–2.119 μm) and with linear polarization, (e) eight wavelength bands (0.340–2.119 μm) and no polarization, and (f) eight wavelength bands (0.340–2.119 μm) and with linear polarization.

However, the process does not go smoothly. For example, the case of $\Phi_{\rm out}=15^\circ/165^\circ$ appears to be sometimes better than $\Phi_{\rm out}=0^\circ/180^\circ$, especially for polarization observations. We think that this is because the finer angular spacing of $\theta_{\rm out}$ with the same number of scattering angles covering a smaller range of scattering angles sometimes can be better than a somewhat coarser angular spacing covering a wider range.

IV. Conclusion

In this paper, we presented the results of the PCA of simulated satellite observations of aerosol over oceans. We modeled various possible observation situations when a satellite sensor can perform multispectral, multiangle, and polarization measurements of the reflected solar radiances. With the PCA, we

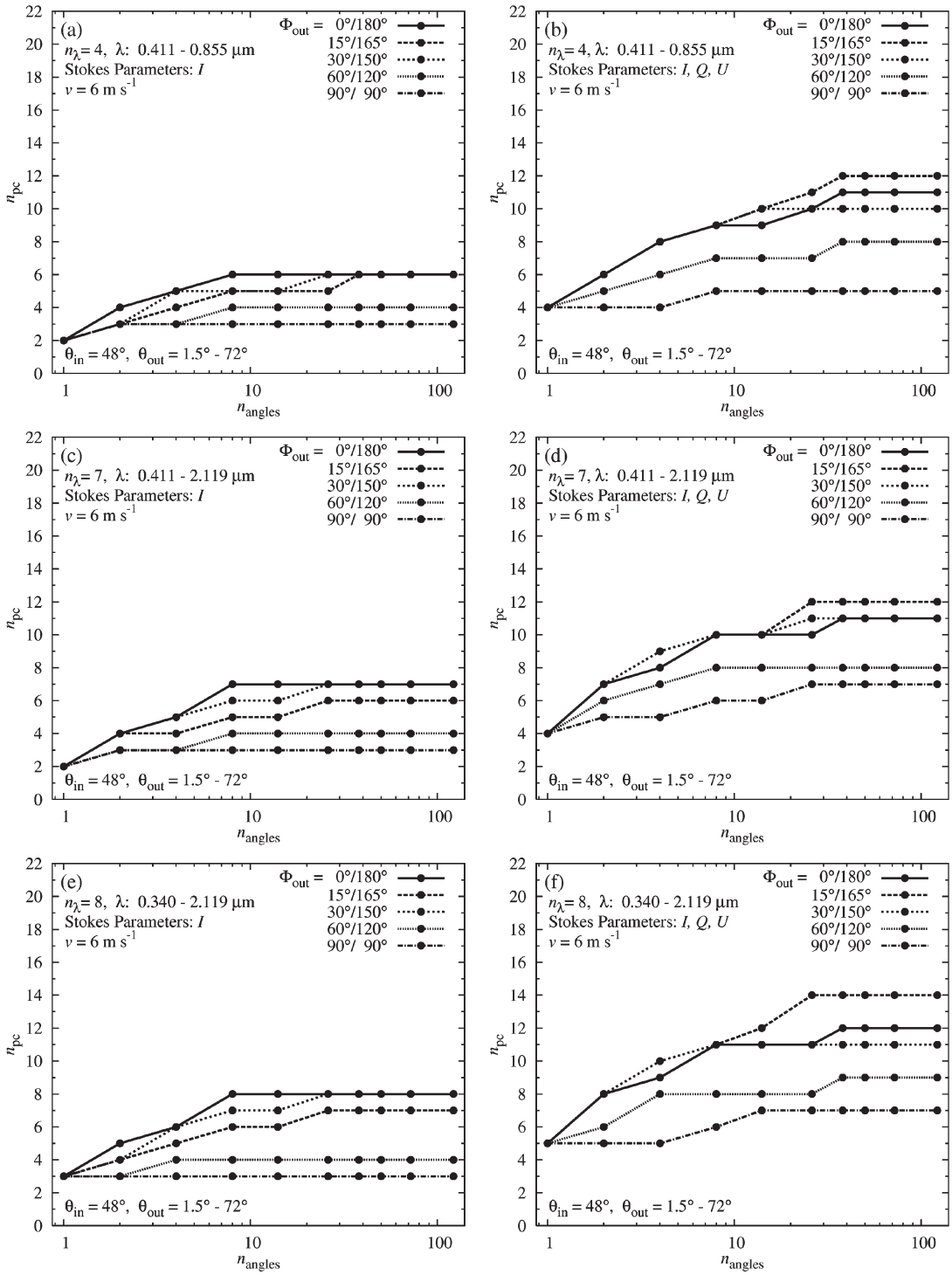

Fig. 4. Number of SPCs as a function of the number of viewing directions for $\theta_{\rm in} = 48°$, $\theta_{\rm out} = 1.5°{-}72°$, and $\Phi_{\rm out} = 0°/180°{-}90°/90°$, and with the wind speed fixed to 6 m $\cdot$ s^{-1} for (a) four wavelength bands (0.411–0.855 μm) and no polarization, (b) four wavelength bands (0.411–0.855 μm) and with linear polarization, (c) seven wavelength bands (0.411–2.119 μm) and no polarization, (d) seven wavelength bands (0.411–2.119 μm) and with linear polarization, (e) eight wavelength bands (0.340–2.119 μm) and no polarization, and (f) eight wavelength bands (0.340–2.119 μm) and with linear polarization.

analyzed the sensitivity of the information contained in the radiances to the following parameters: 1) AOT; 2) SSA of aerosol particles; 3) height of the aerosol layer; 4) aerosol model, which includes the size distribution parameters and optical constants; and (5) wind speed over ocean. To choose the number of SPCs, we used the CPV rule with the critical percentage of 90%, which satisfies all our criteria for the solution: uniqueness, physical sense, and informational sense.

Note, however, that a larger number of eigenvalues that meet the stopping rule does not necessarily mean more information about aerosols. For example, having glint or higher wind speed, or larger field-of-view of the instrument creates greater scene

variance, but not necessarily more information about aerosols, due to the additional information needed to describe the surface.

The principal results of this paper can be summarized as follows.

1) By making observations at one to eight wavelengths across the solar spectrum and one to eight view angles, we can obtain totally up to nine SPCs (no polarization) and up to 12 SPCs (with linear polarization channels), which represent 91%–98% of the information.
2) By adding more wavelength channels from one (0.533 μm) to eight (0.34–2.119 μm), we can receive two to ten extra SPCs overall, one to three extra SPCs due to the linear polarization data comparing with the case of no polarization, up to two extra SPCs due to glint when observations are done in the principal plane, and up to three SPCs relating to the wind speed.
3) By adding more view angles from one to eight ($\theta_{\rm out} = 0^\circ - 72^\circ$), we can get 2–12 extra SPCs overall, up to four extra SPCs due to the linear polarization channels, up to four extra SPCs due to observations in glint compared with the off-glint observations, and up to four SPCs associated with the wind speed.
4) By adding linear polarization channels, we can get additional one to seven SPCs overall, with one SPC due to the wind speed.
5) Our PCA analysis shows that the observations should be most sensitive to aerosol model (size distribution and optical parameters), followed in decreasing order by optical thickness τ, SSA ω_o, and aerosol layer height H. The sensitivity to the wind speed ν depends on the number of view angles.
6) We have studied the behavior of the number of SPCs as a function of the position of the observational plane $\Phi_{\rm out}$ and the number of view angles n_θ. We have found that, with increasing n_θ, there is no systematic increase in the number of SPCs for $n_\theta \geq 10-15$, when no polarization, and for $n_\theta \geq 30$ with linear polarization data. By using a quite large n_θ, we can get from two to ten SPCs without polarization and from 4 to 16 SPCs with linear polarization data. Up to two SPCs should be due to the wind speed.
7) The results of this paper are generally consistent with those of previous PCA study by Tanré *et al.* [24]. For the MODIS-like case with seven wavelength bands 0.411–2.119 μm, one view angle, and no polarization, we received two (for CPV 90% which seems more realistic) or three (for CPV 95%) SPCs, whereas Tanré *et al.* obtained up to two SPCs. Note however that the work [24] used more simplistic assumptions. For example, they modeled radiative transfer through aerosol in the single-scattering approximation.
8) The methodology and results of our PCA can be useful in estimating the reliability of aerosol parameters retrieved from existing and future satellite observations.

ACKNOWLEDGMENT

The authors would like to thank M. Mishchenko (NASA Goddard Institute for Space Studies) for the detailed and constructive comments on an earlier version of this paper and the reviewers for their constructive suggestions that have improved this paper significantly.

REFERENCES

[1] V. Ramanathan, P. J. Crutzen, J. T. Kiehl, and D. Rosenfeld, "Atmosphere–aerosols, climate, and the hydrological cycle," *Science*, vol. 294, no. 5549, pp. 2119–2124, 2001.
[2] Y. J. Kaufman, D. Tanré, and O. Boucher, "A satellite view of aerosols in the climate system," *Rev. Nature*, vol. 419, no. 6903, pp. 215–223, Sep. 2002.
[3] M. O. Andreae, "Climatic effects of changing atmospheric aerosol levels Ch 10," in *World Survey of Climatology*, vol. 16. New York: Future Climates World, 1995, pp. 341–392.
[4] I. Koren, Y. J. Kaufman, L. A. Remer, and J. V. Martins, "Measurement of the effect of Amazon smoke on inhibition of cloud formation," *Science*, vol. 303, no. 5662, pp. 1342–1345, Feb. 2004.
[5] J. Haywood and O. Boucher, "Estimates of the direct and indirect radiative forcing due to tropospheric aerosols," *Rev. Geophys.*, vol. 38, no. 4, pp. 513–543, 2000.
[6] S. A. Twomey, M. Piepgrass, and T. L. Wolfe, "An assessment of the impact of pollution on the global albedo," *Tellus*, vol. 36B, pp. 356–366, 1984.
[7] R. J. Charlson *et al.*, "Climate forcing by anthropogenic aerosols," *Science*, vol. 255, no. 5043, pp. 423–430, Jan. 1992.
[8] J. T. Kiehl and B. P. Briegleb, "The relative roles of sulfate aerosols and greenhouse gases in climate forcing," *Science*, vol. 260, no. 5106, pp. 311–314, Apr. 1993.
[9] J. V. Martins *et al.*, "Effects of black carbon content, particle size, and mixing on light absorption by aerosol particles from biomass burning in Brazil," *J. Geophys. Res.*, vol. 103, no. D24, pp. 32 041–32 050, Dec. 1998.
[10] J. Hansen, M. Sato, and R. Ruedy, "Radiative forcing and climate response," *J. Geophys. Res.*, vol. 102, no. D6, pp. 6831–6864, 1997.
[11] A. S. Ackerman *et al.*, "Reduction of tropical cloudiness by soot," *Science*, vol. 288, no. 5468, pp. 1042–1047, May 2000.
[12] J. Hansen *et al.*, "Earth's energy imbalance: Confirmation and implications," *Sci. Mag.*, vol. 308, no. 5727, pp. 1431–1435, Jun. 2005.
[13] M. Mishchenko *et al.*, "Monitoring of aerosol forcing of climate from space: Analysis of measurement requirements," *J. Quant. Spectrosc. Radiat. Transf.*, vol. 88, no. 1–3, pp. 149–161, Sep. 2004.
[14] M. I. Mishchenko, L. D. Travis, and A. A. Lacis, *Scattering, Absorption, and Emission of Light by Small Particles*. New York: Cambridge Univ. Press, 2002.
[15] P. Y. Deschamps *et al.*, "The POLDER mission: Instrument characteristics and scientific objectives," *IEEE Trans. Geosci. Remote Sens.*, vol. 32, no. 3, pp. 598–615, May 1994.
[16] V. V. Salomonson, W. L. Barnes, P. W. Maymon, H. E. Montgomery, and H. Ostrow, "MODIS: Advanced facility instrument for studies of the Earth as a system," *IEEE Trans. Geosci. Remote Sens.*, vol. 27, no. 2, pp. 145–153, Mar. 1989.
[17] D. J. Diner *et al.*, "MISR: A multiangle imaging spectroradiometer for geophysical and climatological research from EOS," *IEEE Trans. Geosci. Remote Sens.*, vol. 27, no. 2, pp. 200–214, Mar. 1989.
[18] M. I. Mishchenko and L. D. Travis, "Satellite retrieval of aerosol properties over the ocean using polarization as well as intensity of reflected sunlight," *J. Geophys. Res.*, vol. 102, no. D14, pp. 16 989–17 013, 1997.
[19] ——, "Satellite retrieval of aerosol properties over the ocean using measurements of reflected sunlight: Effect of instrumental errors and aerosol absorption," *J. Geophys. Res.*, vol. 102, no. D12, pp. 13 535–13 553, 1997.
[20] M. I. Mishchenko *et al.*, "Retrieving CCN column density from single-channel measurements of reflected sunlight over the ocean: A sensitivity study," *Geophys. Res. Lett.*, vol. 24, no. 21, pp. 2655–2658, 1997.
[21] I. T. Jolliffe, *Principal Component Analysis*, 2nd ed. New York: Springer-Verlag, 2002.
[22] Y. J. Kaufman, R. S. Fraser, and R. A. Ferrare, "Satellite measurements of large-scale air pollution: Methods," *J. Geophys. Res.*, vol. 95, no. D7, pp. 9895–9909, Jun. 1990.
[23] A. Morel, "In-water and remote measurements of ocean color," *Boundary Layer Meteorol.*, vol. 18, no. 2, pp. 177–201, Mar. 1980.
[24] D. Tanré, M. Herman, and Y. J. Kaufman, "Information on aerosol size distribution contained in solar reflected spectral radiances," *J. Geophys. Res.*, vol. 101, no. D14, pp. 19 043–19 060, 1996.

[25] R. C. Levy *et al.*, "Evaluation of the MODIS retrievals of dust aerosol over the ocean during PRIDE," *J. Geophys. Res.*, vol. 108, no. D19, 8594, Jul. 2003. PRD 10-1.
[26] M. Mishchenko *et al.*, "Aerosol retrievals from AVHRR radiances: Effects of particle nonsphericity and absorption and an updated long-term global climatology of aerosol properties," *J. Quant. Spectrosc. Radiat. Transfer*, vol. 79/80, pp. 953–972, Jun–Sep. 2003.
[27] Z. Ahmad and R. S. Fraser, "An iterative radiative transfer code for ocean–atmosphere system," *J. Atmos. Sci.*, vol. 39, no. 3, pp. 656–665, Mar. 1982.
[28] C. Cox and W. Munk, "Statistics of the sea surface derived from sun glitter," *J. Mar. Res.*, vol. 13, pp. 198–208, 1954.
[29] P. Koepke, "Effective reflectance of oceanic whitecaps," *Appl. Opt.*, vol. 23, no. 11, pp. 1816–1823, Jun. 1984.
[30] H. R. Gordon, T. Du, and T. Zhang, "Remote sensing of ocean color and aerosol properties: Resolving the issue of aerosol absorption," *Appl. Opt.*, vol. 36, no. 33, pp. 8670–8684, Nov. 1997.
[31] J. Cadima and I. T. Jolliffe, "Loadings and correlations in the interpretation of principal components," *J. Appl. Stat.*, vol. 22, no. 2, pp. 203–214, 1995.
[32] W. W. Hsieh, "Nonlinear multivariate and time series analysis by neural networks methods," *Rev. Geophys.*, vol. 42, no. 1, RG1003, Mar. 2004.
[33] A. Hyvärinen, J. Karhunen, and E. Oja, *Independent Component Analysis*. Hoboken, NJ: Wiley, 2001.
[34] G. E. Forsythe, M. A. Malcolm, and C. B. Moler, *Computer Methods for Mathematical Computations*. Englewood Cliffs, NJ: Prentice-Hall, 1977.
[35] W. R. Zwick and W. F. Velicer, "Comparison of five rules for determining the number of components to retain," *Psychol. Bull.*, vol. 99, no. 3, pp. 432–442, 1986.
[36] H. F. Kaiser, "The application of electronic computers to factor analysis," *Educ. Psychol. Meas.*, vol. 20, no. 1, pp. 141–151, Apr. 1960.
[37] L. Guttman, "Some necessary conditions for common factor analysis," *Psychometrika*, vol. 19, no. 2, pp. 149–161, 1954.
[38] R. B. Cattell, "The scree test for the number of factors," *Multivariate Behav. Res.*, vol. 1, pp. 245–276, 1966.
[39] R. B. Cattell and S. Vogelmann, "A comprehensive trial of the Scree and KG criteria for determining the number of factors," *Multivariate Behav. Res.*, vol. 12, pp. 289–325, 1977.
[40] M. S. Bartlett, "Tests of significance in factor analysis," *Br. J. Psychol., Stat. Section*, vol. 3, pp. 77–85, 1950.
[41] G. R. North, T. L. Bell, and R. F. Cahalan, "Sampling errors in the estimation of empirical orthogonal functions," *Mon. Weather Rev.*, vol. 110, no. 7, pp. 699–706, Jul. 1982.

Viktor Zubko received the M.S. degree in astrophysics (*with honors*) from Taras Shevchenko State University, Kyiv, Ukraine, in 1979 and the Ph.D. degree in physics from the Ukrainian National Academy of Sciences, Kyiv.

From 1997 to 1999, he was a Visiting Scientist with the Department of Physics, Technion–Israel Institute of Technology, Haifa, Israel. From 2000 to 2001, he was a Research Scholar with the Department of Physics and Astronomy, University of Kentucky, Lexington. From 2001 to 2004, he was a Research Scientist with the NASA Goddard Space Flight Center (GSFC). From 2004 to 2006, he worked as a Senior Scientific Analyst with Nortel Government Solutions, Inc., Lanham, MD. He is currently an Atmospheric Scientist with RS Information Systems, Inc./Goddard Earth Sciences Data and Information Services Center, NASA GSFC, Greenbelt, MD. His experience includes theory and modeling of atmospheric aerosols and cosmic dust, polarized radiative transfer, light scattering by small particles, remote sensing of aerosols, numerical inversion techniques for ill-posed problems, principal component analysis, and scientific programming. He is currently working on the modeling of 3-D radiative transfer of solar-scattered radiation in clouds and on the effect of aerosol on cloud optical properties.

Dr. Zubko is a Full Member of the American Astronomical Society.

Yoram J. Kaufman received the B.S. and M.S. degrees in physics from the Technion–Israel Institute of Technology, Haifa, Israel, and the Ph.D. degree from Tel-Aviv University, Tel Aviv, Israel.

He has served as the Project Scientist of the Earth Observing System first satellite EOS-Terra, from 1996 through its launch in December 1999, and was a member of the MODIS Science Team (1988–2003). He came to NASA Goddard Space Flight Center (GSFC), Greenbelt, MD, in 1979 on an NRC Fellowship Award. Until his death in May 2006, he was a Senior Fellow and Atmospheric Scientist with the GSFC. His recent work included theoretical and experimental research in atmospheric radiative transfer and remote sensing of aerosols, their interaction with clouds and radiation, and impact on climate. He conducted the Smoke/sulfate, Clouds and Radiation (SCAR) field experiments in Brazil and the U.S. (1993–1995) to characterize smoke aerosol properties, their emissions from fires, and their effect on clouds and radiation. He has over 150 refereed publications.

Dr. Kaufman was the seventh recipient of the NASA/GSFC Nordberg Award for Earth Sciences and was awarded the NASA Medal for Exceptional Scientific Achievement. He was a Fellow of the American Meteorological Society and is listed among the ISI highly cited scientists in Geophysics. He died on May 31, 2006.

Richard I. Burg received the B.S. degree in physics from Stony Brook University (SUNY), Stony Brook, NY, in 1978 and the Ph.D. degree in physics from the Massachusetts Institute of Technology, Cambridge, in 1986.

He is presently a NASA Chief Engineer at the NASA Goddard Space Flight Center (GSFC), Greenbelt, MD. He was the Project Manager for the Glory Mission and for the Next Generation Space Telescope (NGST) (now the James Webb Space Telescope). He was also a Mission Architect, a Program Technologist, and the Manager of the NGST Optical Telescope Element. Before coming to NASA GSFC, he was an Astrophysicist with the Johns Hopkins University. He was a Postdoctoral Fellow with the Space Telescope Science Institute. He has conducted research on spectroscopic classification of galaxies, galaxy clusters, the X-ray background, and X-ray optics. He has also worked on developing concepts for nulling interferometers for planet finding.

J. Vanderlei Martins received the B.Sc., M.Sc., and Ph.D. degrees in physics from the Institute of Physics, University of São Paulo (USP), São Paulo, Brazil.

He joined the Group of Studies of Air Pollution, Institute of Physics (USP), in 1990 and conducted research in environmental and atmospheric applied physics, developing nuclear analytical techniques using particle accelerators for material analysis, including aerosols and tree rings. He has participated in several ground-based and aircraft field experiments studying properties of aerosols from biomass burning, urban, and biogenic emissions, as well as their effects on clouds and radiation. In 2000, he joined the MODIS aerosol group, NASA Goddard Space Flight Center, Greenbelt, MD, through the Joint Center for Earth Systems Technology (JCET-UMBC), and in 2001, he was elected as a representative member of the International Radiation Commission where he serves to this date.